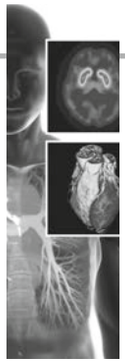

MRI of atherosclerosis: from mouse to man

Atherosclerosis and its thrombotic complications still remain the major cause of morbidity and mortality in western societies. Atherogenesis in humans generally occurs over decades, and lesion evolution and growth may vary according to heredity, gender, lifestyle and environmental conditions. However, the development of animal models of experimental atherosclerosis and the emergence of several imaging modalities have provided indispensable knowledge to our understanding of the fundamental mechanisms of disease progression and allowed the *in vivo* detection of atherosclerosis in animals and humans. MRI has evolved as one of the leading noninvasive imaging modalities to visualize the vessel wall with high spatial resolution and without ionizing radiation. This article summarizes the currently available animal models of experimentally induced atherosclerosis and the application of MRI in preclinical and clinical imaging studies.

KEYWORDS: animal model ▪ atherosclerosis ▪ contrast agent ▪ molecular imaging ▪ MRI ▪ thrombosis

Alkystis Phinikaridou* & René M Botnar

Division of Imaging Science & Biomedical Engineering, King's College London, The Rayne Institute, 4th Floor, Lambeth Wing, St Thomas' Hospital, London SE1 7EH, UK
**Author for correspondence:*
Tel.: +44 207 188 8386
Fax: +44 207 188 5442
alkystis.1.phinikaridou@kcl.ac.uk

Atherosclerosis is a progressive arterial disease characterized by intimal thickening from the accumulation of lipids [1], smooth muscle cells, lipid-filled macrophages, monocytes, lymphocytes, erythrocytes, platelets [2–4] and extracellular matrix proteins (collagen, elastin, proteoglycans) [5,6]. It is considered the major contributor to the development of cardiovascular disease, the leading cause of death in the USA [7] and worldwide [8].

Histological studies using excised human vessels and atherosclerotic animal models have provided valuable information regarding the pathophysiology of atherosclerosis and thrombosis. Human vessels collected at autopsy were used by the American Heart Association Committee on Vascular Lesions to stratify the severity of atherosclerotic plaques based on compositional and morphological criteria [9–11]. This classification system was later modified by Virmani *et al.* [12]. It has also been shown that acute cardiovascular events and sudden death related to atherosclerosis are due to disruption of vulnerable or high-risk plaques and subsequent thrombosis, which may quickly cause luminal occlusion. Conversely, stable plaques can remain clinically asymptomatic. Currently, three distinct histological features: plaque rupture, plaque erosion and calcified nodules, have been associated with luminal thrombosis. Ruptured human plaques, also termed thin-cap atheromas, usually have:

- A thin (<65 µm in the coronary arteries) [13–15], inflamed [16,17] fibrous cap infiltrated by macrophages;
- A large lipid core (>40% of the total lesion area);
- Increased neovessels [18];
- Medial and adventitial disorganization [19];
- Intraplaque hemorrhage [20];
- Positive/outward vessel wall remodeling [21].

Unlike plaque rupture, in eroded plaques the thrombus forms over an intima lacking endothelial cells and a fibrous cap rich in smooth muscle cells, proteoglycans and type 3 collagen fibers [22]. Finally, atherothrombi may also occur as a result of calcified nodules that bulge into the lumen through a disrupted fibrous cap [12].

Despite the incremental understanding of the pathophysiology of atherosclerosis, histological studies are limited by their retrospective nature. Several studies have shown the feasibility of both invasive (angiography, angioscopy, intravascular ultrasound [IVUS], optimal coherence tomography, thermography, Raman spectroscopy, near-infrared spectroscopy) and noninvasive (B-mode ultrasound tomography, CT, PET, MRI) imaging modalities for *in vivo* vessel wall imaging and characterization of atherosclerosis. Of these techniques, angiography and IVUS have been widely used in clinical practice primarily to estimate the degree of luminal stenosis and stratify patients in different intervention groups. However, angiographic studies of coronary arteries, performed before and after nonfatal myocardial infarction, showed that at

Future Medicine part of fsg

Table 1. Animal models used in the study of atherosclerosis.

Species	Characteristics and use	Ref.
Mammalian nonprimate		
Mice C57BL/6, C3H, BALB/c	The C57BL/6 is the most susceptible strain, the BALB/c has intermediate susceptibility and C3H has the least susceptibility C57BL/6 mice develop small lesions in the aortic root characterized by lipid-laden macrophages when fed a hyperlipidemic diet for prolonged periods. With further feeding they also develop lesions with cellular debris and collagen	[163,164]
ApoB transgenic mice	Develop foam cell-rich lesions when fed a diet enriched in saturated fat and cholesterol	[165]
ApoE$^{-/-}$	Spontaneous lesions form even when the animals are fed a standard chow diet low in fat and free of cholesterol. Lesions rich in foamy macrophages form in the proximal aorta by 3 months of age and more complex lesions develop by 8–9 months	[166–168]
	Lesion formation can be significantly accelerated with high-cholesterol HFD. Advanced lesions with fibrous cap, small necrotic cores and lipid deposits form by 3 months of HFD. Lesions are found in the aortic root, the aortic arch, the brachiocephalic artery, the base of the left carotid and the left subclavian arteries and the renal area	[169,170]
	Carotid atherosclerosis was induced by using HFD and perivascular constrictive collars. This model was used to study the effects of shear stress on plaque progression and morphology	[171,172]
ApoE*3-Leiden (E3L) transgenic mice	Develop lesions when the animals are fed a high-fat, high-cholesterol diet. Lesions contained smooth muscle cells, macrophages and T lymphocytes	[173]
LDLR$^{-/-}$	Develop foamy lesions when fed an atherogenic diet containing cholesterol, saturated fat and cholate	[174]
LDLR$^{-/-}$/ApoBEC$^{-/-}$	A model of human familial hypercholesterolemia	[175]
LDLR$^{-/-}$/ApoB$^{+/+}$	Exhibit accelerated atherosclerosis on a chow diet. Develop large, complex, lipid-laden atherosclerotic lesions	[176]
LDLR$^{-/-}$/ApoCIII	A model of familial combined hyperlipidemia. Lesions form when the animals are fed an atherogenic diet	[177]
ApoE$^{-/-}$/LDLR$^{-/-}$	Develop foamy lesions when fed an atherogenic diet containing cholesterol, saturated fat and cholate	[178]
ApoE$^{-/-}$/C1039G$^{-/+}$	Hypercholesterolemia with a mutation in the *fibrillin-1* gene leading to impaired elastogenesis promotes features of plaque instability	[179]
ApoE$^{-/-}$/MMP1$^{-/-}$	Develop lesions when fed a high-cholesterol HFD. Surprisingly, the lesions are less advanced	[180]
ApoE$^{-/-}$/eNOS$^{-/-}$	Develop accelerated atherosclerosis, aortic aneurysm formation and ischemic heart disease after 16 weeks of high-cholesterol HFD	[181]
ApoE$^{-/-}$/iNOS$^{-/-}$	Develop reduced atherosclerosis and have lower plasma lipid peroxides	[182]
ApoE$^{-/-}$/Ncp1$^{-/-}$	Develop lesions increased in size and extensive medial degradation. The lesions showed signs of spontaneous plaque disruption with overlay thrombus	[183]
Rats	Not a preferred model for studying atherosclerosis. Very resistant to the development of atherosclerosis even when fed with high-cholesterol diets that induce lesions in other species. Induction of atherosclerosis was achieved with a combination of extremely high lipid content coupled to auxiliary procedures such as bile acid supplementation, vascular injury, thyroid destruction and perinephritis	[184,185]
Rabbits	Susceptible, especially the NZW rabbits, to diet-induced atherosclerosis and the type of lesions depend on the duration and composition of the atherogenic diet. Atherosclerotic plaques range from early to advanced/complicated lesions depending on the induction method	[1,186]
	Rabbits developed foam cell-rich (fatty steaks) plaques when short-term HFDs (6–10 weeks) were the only stimulus used to induce atherosclerosis. However, intermittent cycles of high-cholesterol feeding with periods of normal diet (2 months of high-cholesterol diet, followed by 2–3 months of normal diet, followed by another cycle of high-cholesterol diet for 2 months and normal diet for 2 months) induced plaques at more advanced stages that resembled human atheroma. Moreover, with the combination of arterial wall injury and hyperlipidemia, advanced lesions form in shorter periods	[187–191]
	WHHL rabbits serve as models of homozygous familial hypercholesterolemia. They develop a variety of lesions under normal chow and have been used to study lipoprotein metabolism owing to the elevation of LDLs	[192–195]

HFD: High-fat diet; IDL: Intermediate-density lipoprotein; LDL: Low-density lipoprotein; MMP: Matrix metalloproteinase; NZW: New Zealand white; VLDL: Very low-density lipoprotein; WHHL: Watanabe heritable hyperlipidemic.

Table 1. Animal models used in the study of atherosclerosis (cont.).

Species	Characteristics and use	Ref.
Mammalian nonprimate		
Rabbits (cont.)	St Thomas' strain of familial combined hyperlipidemia develops atherosclerotic lesions on a standard chow diet and are characterized by elevated lower-density lipoproteins (VLDL, IDL, LDL)	[196]
	Jackson Laboratory AX/JU strains are hyper-responsive to dietary cholesterol	[197]
	Jackson Laboratory IIIVO/ JU strain is hyporesponsive to dietary cholesterol	[198,199]
	Transgenes of different human apolipoproteins have been expressed in NZW and WHHL rabbits for the study of lipoprotein metabolism	[199]
	Transgenic rabbit model of MMP-12 in atherosclerosis was used to study the effects of MMP in plaque formation and progression	[200]
Swine	Susceptible to dietary induced atherosclerosis. Lesions occur in both the aorta and branch vessels. The size of heart and vessels is sufficient for studies of cardiovascular function, ischemic heart disease and for developing new diagnostic and surgical procedures	[201–204]
	Yucatan miniature swine breed is also susceptible to high-fat, high-cholesterol, diet-induced atherosclerosis with and without the presence of diabetes	[204–206]
	Diabetes in conjunction with hyperlipidemia was used in Yorkshire swine to accelerate atherosclerosis	[207]
	Genetic mutations affecting the structure of plasma lipoproteins or the LDL receptor have been used to induce hypercholesterolemia and atherosclerosis in the coronary arteries	[208–210]
	A familial hypercholesterolemic downsized pig with human-like coronary atherosclerosis has been proposed as a model for preclinical studies	[211]
Dogs	Cholesterol feeding and thyroid inactivation for a year (using thiouracil) are needed to induce advanced lesions	[212]
	Addition of butter in cholesterol–thiouracil diet accelerates disease progression and foamy lesions form by 8 weeks	[213]

HFD: High-fat diet; IDL: Intermediate-density lipoprotein; LDL: Low-density lipoprotein; MMP: Matrix metalloproteinase; NZW: New Zealand white; VLDL: Very low-density lipoprotein; WHHL: Watanabe heritable hyperlipidemic.

the site of thrombosis, the pre-existing lesion frequently resulted in less than 50% stenosis [23,24] and frequently did not cause angina or a positive treadmill test. Only 20% of acute complete occlusions occur in lesions with a stenosis greater than 75% [25].

Therefore, there is a need for the development of a noninvasive imaging modality that would allow not only the estimation of luminal stenosis but also a compositional characterization of atherosclerotic plaque. This review article will focus on the different animal models currently available for studying atherosclerosis and the applications of noncontrast-enhanced, contrast-enhanced and molecular MRI for preclinical and clinical use.

Animal models of atherosclerosis: advantages & disadvantages

The complexity and slow progression of atherosclerosis in humans and the unpredictable nature of plaque disruption have necessitated the development of animal models for understanding the molecular and cellular pathways involved in disease progression and the clinical manifestations, as well as the development of diagnostic procedures and therapeutic interventions. Unlike in humans, animal models allow the development of the disease in a reasonable time span and under precise settings where environmental, genetic and dietary variables can be controlled. Furthermore, animals allow the evaluation of risk factors independently or in combinations, in the presence or absence of other intercurrent diseases. Many requirements need to be satisfied in order to make an animal model suitable for the study of atherosclerosis. Some of the factors include: strain availability, susceptibility to disease, ease in handling, breeding and maintenance cost, reproducibility of results, anatomical, morphological and biochemical similarities to the human disease.

Anitschkow and Chalatow were among the first researchers to induce experimental atherosclerosis in animals by feeding rabbits an enriched cholesterol diet [1,26]. Since then, several other experimental conditions have been used to induce lesions in different animal species including dietary, physical, chemical, immunological and transgenic approaches applied individually or in combinations, simultaneously or sequentially. A summary of the different animal models available for studying atherosclerosis together with their basic characteristics and uses is illustrated in Table 1.

Table 2. *In vivo* MRI of atherosclerosis in animal models.

Animal model	Vessel	Target	Contrast agent	Ref.
Mice				
ApoE$^{-/-}$	Abdominal aorta and iliac arteries	None	Non-CE	[36]
ApoE$^{-/-}$	Aorta	None	Non-CE	[37]
ApoE$^{-/-}$	Thoracic aorta	None	Non-CE	[38]
ApoE$^{-/-}$	Aortic root	None	Non-CE	[39]
ApoE$^{-/-}$	Plaque regression in the thoracic aorta	None	Non-CE	[40]
ApoE$^{-/-}$	Injury-induced neointima formation in the carotid artery	None	Non-CE	[41]
ApoE$^{-/-}$	Abdominal aorta	None	P717, gadolinium-based blood pool agent	[214]
ApoE$^{-/-}$	Aortic arch	None	P792 (Vistarem™), gadolinium-based blood pool agent	[215]
ApoE$^{-/-}$	Aortic arch and aortic root	VCAM-1	Multimodal nanoparticles	[84,85]
ApoE$^{-/-}$	Abdominal aorta	Macrophage scavenger receptor	Gadolinium-loaded immunomicelles and bimodal PEG-micelles	[106,107]
ApoE$^{-/-}$	Abdominal aorta	Oxidation-specific epitopes	Gadolinium-loaded micelles	[114]
ApoE$^{-/-}$	Aortic root *ex vivo*	VCAM-1 and P-selectin	MPIO	[86]
ApoE$^{-/-}$	Abdominal aorta	MMP	P947 gadolinium based	[150]
ApoE$^{-/-}$	Aortic arch	Lipoproteins	LDL-based nanoparticles (GdDO3A-OA-LDL)	[112]
ApoE$^{-/-}$	Abdominal aorta	Lipoproteins	HDL-based nanoparticles	[110,111]
ApoE$^{-/-}$	Brachiocephalic	Elastin	Small molecular weight gadolinium-based peptide	[148]
ApoE$^{-/-}$	Aortic arch and abdominal aorta	Annexin-5	Gadolinium-loaded micelles	[152]
ApoE$^{-/-}$	Brachiocephalic	None	SPIO	[98]
ApoE$^{-/-}$/eNOS$^{-/-}$	Abdominal aorta	Cannabinoid receptor and NGAL	Gadolinium-loaded micelles	[108,109]
LDLR$^{-/-}$	Brachiocephalic	None	Non-CE	[216]
LDLR$^{-/-}$/LOX-1$^{-/-}$	Aortic root and arch	LOX-1	Gadolinium labeled LOX-1 antibody	[113]
C57/B6J	Carotid thrombi	α2-antiplasmin	Bimodal α2-antiplasmin	[147]
Rabbits				
NZW	Abdominal aorta and thrombosis	None	Non-CE	[42–50]
WHHL	Abdominal aorta	None	Non-CE	[51]
NZW	Coronary arteries	None	Non-CE	[52]
NZW and WHHL	Abdominal aorta	None	Gadofluorine-M (blood pool agent)	[217–221]
WHHL	Abdominal aorta	None	Gadopentetate dimeglumine	[121]
NZW	Abdominal aorta	None	Gadopentetate dimeglumine	[120,122]
NZW	Abdominal aorta thrombi associated with plaque disruption	Fibrin	EP-2104R	[134]
NZW	Carotid artery thrombi (external injury and stasis)	Fibrin	EP-2104R	[222]
NZW	Abdominal aorta	MMP	P947 is gadolinium-based	[223]
NZW	Abdominal aorta	Blood albumin	Gadofosveset	[126]
NZW	Abdominal aorta	Blood albumin	B-22956/1	[224]
NZW	Abdominal aorta	MPO	Bis-5HT-DTPA(Gd)	[151]
NZW	Abdominal aorta	Angiogenesis	$\alpha_v\beta_3$-integrin-targeted nanoparticles	[123,124]
NZW	Thoracic aorta	None	USPIO	[88]

CE: Contrast enhanced; HDL: High-density lipoprotein; LDL: Low-density lipoprotein; LDLR: Low-density lipoprotein receptor; MION: Monocrystalline iron oxide nanoparticle; MMP: Matrix metalloproteinase; MPIO: Microparticles of iron oxide; MPO: Myeloperoxidase; NZW: New Zealand white; PEG: Polyethylene glycol; SPIO: Superparamagnetic iron oxide particles; SPION: Superparamagnetic iron oxide nanoparticle; USPIO: Ultrasmall superparamagnetic iron oxide particles; WHHL: Watanabe heritable hyperlipidemic.

Table 2. *In vivo* MRI of atherosclerosis in animal models (cont.).

Animal model	Vessel	Target	Contrast agent	Ref.
Rabbits (cont.)				
NZW and WHHL	Abdominal aorta	None	USPIO	[89–92]
NZW	Iliofemoral artery	None	USPIO	[93]
WHHL and NZW	Thoracic aorta Abdominal aorta	None	MION-47	[94,95]
WHHL	Abdominal aorta	None	SPIONs	[96]
Chinchilla bastard	Stagnation thrombi in the external jugular veins	None	USPIO	[97]
Swine				
Yorkshire albino	Coronary	None	Non-CE	[53]
Yucatan	Aorta and Iliac	None	Motexafin gadolinium	[225]
Danish Landrace	Coronary	Blood albumin	Gadofosveset	[83]
Landrace	Coronary	Elastin	BMS-753951	[149]
Domestic	Jugular veins clots	Fibrin	RGD-USPIO	[137]
Domestic	Coronary and pulmonary thrombosis	Fibrin	EP-2104R	[138–142]
Guinea	Carotid artery thrombosis (external injury and stasis)	Fibrin	EP-2104R	[143]

CE: Contrast enhanced; HDL: High-density lipoprotein; LDL: Low-density lipoprotein; LDLR: Low-density lipoprotein receptor; MION: Monocrystalline iron oxide nanoparticle; MMP: Matrix metalloproteinase; MPIO: Microparticles of iron oxide; MPO: Myeloperoxidase; NZW: New Zealand white; PEG: Polyethylene glycol; SPIO: Superparamagnetic iron oxide particles; SPION: Superparamagnetic iron oxide nanoparticle; USPIO: Ultrasmall superparamagnetic iron oxide particles; WHHL: Watanabe heritable hyperlipidemic.

MRI of atherosclerosis in animal models & humans

Over the last decades extensive research has been dedicated to developing MR methods for *in vivo* imaging of atherosclerosis in animal models and humans. The major applications of MRI in characterizing animal and human atherosclerosis are described below and are summarized in Tables 2 & 3.

■ Assessment of plaque burden & composition

MRI has been applied to characterize plaque composition on the basis of biophysical and biochemical factors (T_1 and T_2 relaxation times), proton density, physical state, molecular motion, fibrous protein content (magnetization transfer) and diffusion coefficients (diffusion-weighted imaging) both *in vivo* and *ex vivo* [27–34]. In addition, *in vivo* techniques such as the black-blood pulse sequence and the use of phased-array receiver coils have improved the delineation of the arterial lumen from the vascular wall, which is critical for lesion visualization [35]. Validation studies were first performed in experimental models including mice [36–41], cholesterol-fed rabbits [42–52] and pigs [53]. In humans, validation of the *in vivo* MRI findings was performed mainly by using *ex vivo* carotid endarterectomy specimens. Several studies showed that the combination of multiple MR contrast weightings (proton density, T_1-weighted, T_2-weighted and time of flight) can be used to identify plaque components [54–59] based on their relative signal intensities and relaxation times. Multicontrast *in vivo* MRI has been used to evaluate plaque size [60] and components including the lipid core, fibrous cap, calcification [54,55,61–64], intraplaque hemorrhage [65,66] as well as features associated with symptomatic human carotid plaques [67]. Furthermore, diffusion-weighted imaging is another technique used to generate contrast between plaque components based on the characteristic diffusion coefficients of water in each tissue [68,69]. Lastly, magnetization transfer between restricted and free-water protons was also used to discriminate the collagenous fibrous cap and the media from the lipid core and adventitia [70].

Several contrast agents have been used to improve the conspicuity of atherosclerotic plaques. Contrast-enhanced MRI using gadolinium diethylenetriamine penta-acetic acid (Gd-DTPA) has been used to increase the sensitivity of MRI and further improve the identification of plaque components. Gd-DTPA has been used for the discrimination between the fibrous cap and the lipid core [71–73] and the visualization of coronary atherosclerosis [74–76].

MRI and MR angiography of coronary arteries still remains challenging owing to cardiac motion, the small caliber and the tortuous structure of the vessels. However, advanced pulse sequence

Table 3. MRI of atherosclerosis in humans.

Vessel	Target	Contrast agent	Ref.
Carotid	None	Non-CE	[60–65,67,73,226–239]
Carotid	None	Gadopentetate dimeglumine	[71,115,116,118,240–244]
Carotid	None	Gadofosveset	[125]
Carotid	None	USPIO	[99–105]
Carotid	None	Non-CE, direct thrombus imaging	[131,245]
Carotid/aorta	Fibrin	EP-2104R, thrombus imaging	[144]
Aorta	None	Non-CE	[246–249]
Aorta	None	Gadopentetate dimeglumine	[72]
Coronary			
MRI	None	Non-CE	[35,156,250–254]
MRI	None	Gadopentetate dimeglumine	[74–76]
MRI	None	Non-CE, direct thrombus imaging	[255]
MRA	None	Non-CE	[77–81]
MRA	None	MS-325/AngioMARK (intravascular agent)	[256]

CE: Contrast enhanced; MRA: Magnetic resonance angiography; USPIO: Ultrasmall superparamagnetic iron oxide particles.

design with navigator gating, with and without breath-holds, has allowed the visualization of the coronary lumen and vessel wall [77–86]. For example, coronary MRI of asymptomatic Type 1 diabetics revealed greater coronary plaque burden in subjects with nephropathy compared with those with normoalbuminuria (Figure 1) [82].

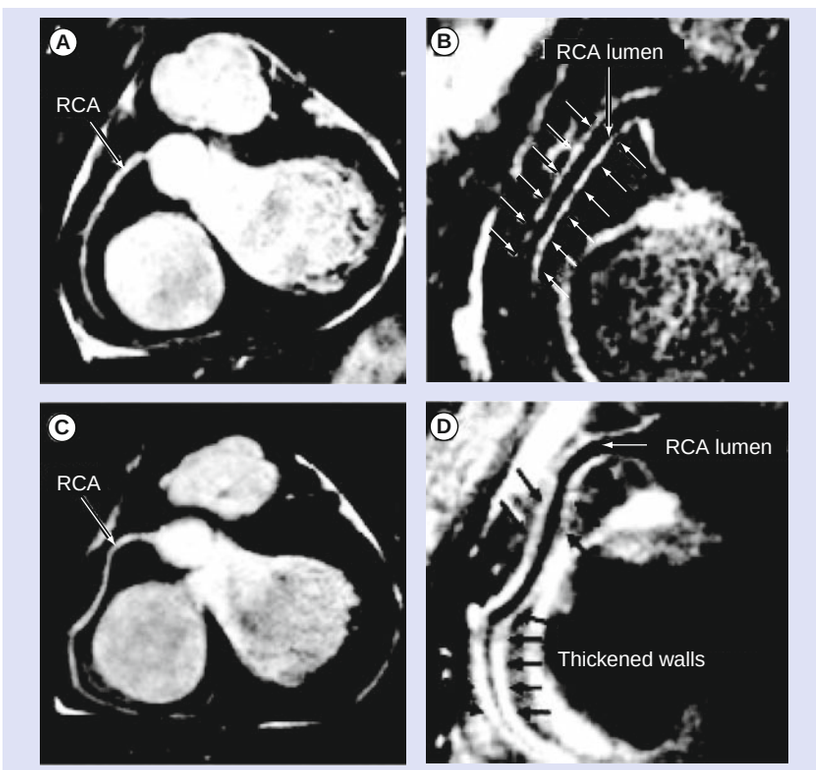

Figure 1. MRI and MR angiography of coronary arteries in patients with Type 1 diabetes. 3D reformatted coronary MRI of the proximal RCA in two subjects without coronary luminal stenosis: a 58-year-old man with long-standing Type 1 diabetes and normoalbuminuria **(A)** and a 44-year-old man with long-standing Type 1 diabetes and diabetic nephropathy. **(C)** The corresponding 3D black-blood vessel wall scans show no cardiovascular MRI evidence of atherosclerotic plaque; **(B)** average and maximum vessel wall thickness (1.1 and 1.3 mm, respectively) and an increased atherosclerotic plaque burden; **(D)** average and maximum vessel wall thickness (2.3 and 3.0 mm, respectively). The anterior and posterior RCA walls are indicated by arrows [82].
RCA: Right coronary artery.

■ Assessment of endothelial activation & permeability

Increase in endothelial permeability and upregulation of adhesion molecules (VCAM-1, ICAM-1, P-selectin) on the endothelial surface occurs in the early stages of atherosclerosis. Increased endothelial leakage allows blood molecules such as low-density lipoprotein (LDL) particles to passively diffuse into the vessel wall whereas expression of adhesion molecules is responsible for the receptor-mediated recruitment of leukocytes. Recently, gadofosveset, a gadolinium-based agent that reversibly binds to blood albumin has been shown to be associated with damaged endothelial cells in a swine model of coronary injury (Figure 2) [83]. Furthermore, multimodal nanoparticles (VIPN-28) [84,85] and microparticles of iron oxide [86] targeting the VCAM-1 receptor and/or P-selectin have been used to image activated endothelium in mouse atherosclerotic plaques. Interestingly, a recent study showed that plaque permeation by contrast agents was strongly dependent on particle size [87].

■ Assessment of plaque macrophages & lipoproteins

Macrophages are key players in the initiation, progression and complication of atherosclerosis. Superparamagnetic iron oxide particles of different sizes stabilized with

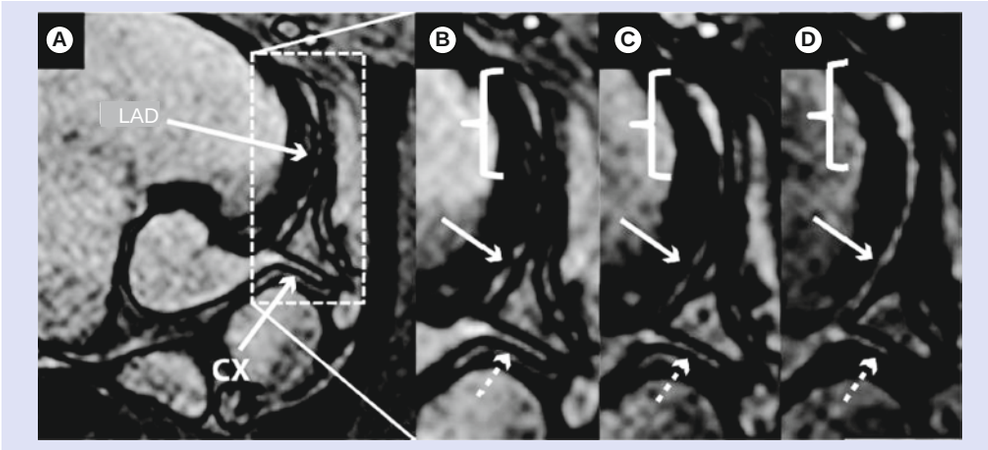

Figure 2. Contrast-enhanced MRI using gadofosveset in a swine model of coronary artery injury. Coronary bright-blood cardiovascular MR angiography **(A)**. T_1-weighted inversion recovery at 5 min **(B)**, 15 min **(C)** and 25 min **(D)** following intravenous administration of gadofosveset. The area of the balloon injured LAD2 segment expands over time indicating time-dependent extravasation of contrast, whereas the intact LAD1 segment (arrow) and CX (dotted arrow) remain constant [83].
CX: Circumflex artery; LAD: Left anterior descending coronary artery.

different surface-coating materials (e.g., dextran or citrate) have been used to estimate the macrophage content of atherosclerotic plaques by becoming nonspecifically endocytosed by macrophages in hyperlipidemic rabbits [88–97], mice [98] and human carotid plaques [99–105]. Macrophages have also been imaged by using gadolinium-loaded micelles targeting the macrophage scavenger receptor in mouse plaques [106,107]. Atherosclerotic plaque macrophages also express the peripheral cannabinoid receptor (CB2-R) and promote fibrous cap degradation by secretion of NGAL. CB2-R- and NGAL-targeted gadolinium-loaded micelles were shown to enhance murine atherosclerotic plaques with a vulnerable phenotype [108,109]. Gadolinium-loaded recombinant high-density lipoprotein-like nanoparticles [110,111] and LDL-based nanoparticles (GdDO3A-OA-LDL) [112] have also been developed to image atherosclerosis in mice. Furthermore, LOX-1 and oxidized plaque LDL particles have been imaged using antibodies that bind to LOX-1 receptor [113] and oxidation specific epitopes [114], respectively.

■ Assessment of plaque neovascularization

Aoki *et al.* were the first to observe a band of enhancement corresponding to the outer vessel wall, after injection of Gd-DTPA, which was attributed to angiogenesis of the wall itself [115]. Enhancement of the outer rim was minimal in early phases of the disease and gradually increased. Subsequently, several other studies have demonstrated a correlation between Gd-DTPA uptake and plaque neovascularization, inflammation, endothelial permeability and fibrosis both in human [74,76,116–119] and animal models [117,120–122]. Gadolinium-based nanoparticles that target $\alpha_v\beta_3$ integrins have also been

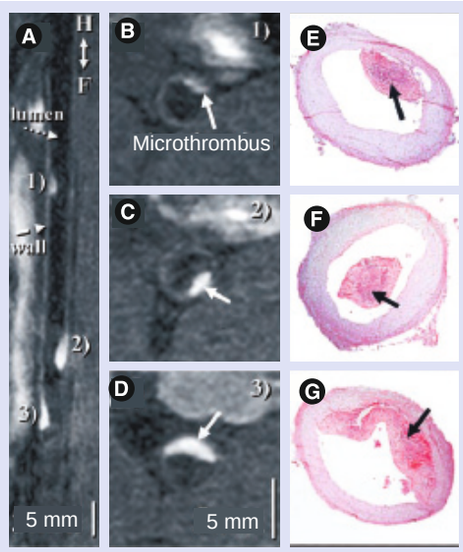

Figure 3. *In vivo* molecular imaging of thrombosis associated with plaque disruption in the rabbit aorta using a fibrin-binding MRI contrast agent. (A) Reformatted view24 of a coronal 3D dataset shows subrenal aorta 20 h after EP-1873 administration. Three well-delineated mural thrombi (arrows) can be observed, with good contrast between thrombus (numbered), arterial blood (dotted arrow) and vessel wall (dashed arrow). The in-plane view of the aorta allows simultaneous display of all thrombi, showing head, tail, length and relative location. **(B–D)** Corresponding cross-sectional views show good agreement with histopathology **(E–G)** [134].

engineered to selectively image plaque angiogenesis and as vehicles for antiangiogenic drug delivery in rabbit aortas [123,124]. Recently, the uptake of gadofosveset was shown to correlate with neovessel density in human carotid [125] and rabbit aortic plaques [126].

■ Assessment of plaque intraplaque hemorrhage & thrombus

Intraplaque hemorrhage and thrombosis are major components of plaque vulnerability. Most MRI studies have focused on the detection of hematoma [127,128], venous thrombosis [129,130], intraplaque hemorrhage [131] and arterial thrombi [132,133] based on the temporal changes of T_1 and T_2 relaxation of different oxygenation states of hemoglobin in erythrocytes. Subsequently, the conspicuity of thrombi has been significantly increased by using fibrin- (Figure 3; rabbit model) [134–144], platelet- [97,145,146] and α2-antiplasmin-targeting contrast agents [147].

■ Assessment of plaque extracellular matrix

The fine-tuned balance in the production and degradation of extracellular matrix proteins (collagen, elastin, proteoglycans) is essential for plaque development and stability. Recently, with the development of a small molecular weight, gadolinium-based, elastin-targeting contrast agent, MRI of the vessel wall at all stages of atherosclerosis has become feasible in mouse atherosclerotic plaques (Figure 4) [148] and in a swine model of coronary injury [149].

■ Assessment of plaque enzymatic activity & apoptosis

Activated matrix metalloproteinases degrade the extracellular matrix and weaken the fibrous cap leading to plaque vulnerability. *In vivo* and *ex vivo* MRI for the characterization for matrix metalloproteinase-rich plaques was achieved with the use of a gadolinium-based matrix metalloproteinase-sensitive MRI contrast (P947) [150].

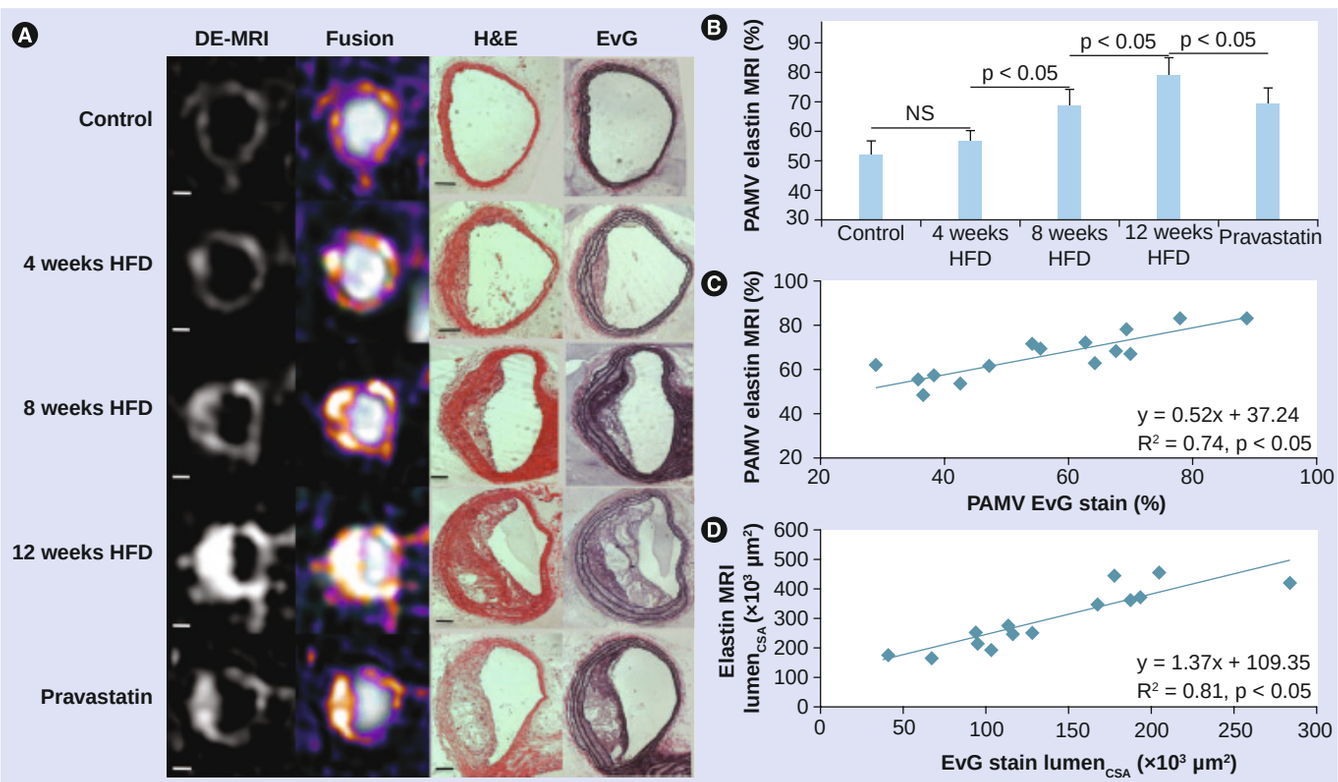

Figure 4. *In vivo* assessment of plaque burden by morphometric measurements. (A) Cross-sectional views of brachiocephalic arteries by MRI of control and ApoE$^{-/-}$ mice 4, 8 and 12 weeks after the onset of HFD (n = 8 per group). High-resolution DE images overlaid on time-of-flight images with corresponding sections from histology (H&E and EvG stain). **(B)** Comparison of average PAMV, calculated from morphometric measurement on high-resolution DE images after the injection of elastin-specific MR contrast agent (n = 8 per group). **(C & D)** Scatter plots showing significant ($p < 0.05$) correlation between morphometric PAMV measurements **(C)** and lumen cross-sectional area measurements **(D)** on high-resolution DE-MRI images and on corresponding EvG-stained histological sections (n = 15). Scale bars: white, 250 µm; black, 100 µm. Values are expressed as means ± standard deviation [148].
DE: Delayed enhancement; EvG: Elastic van Gieson; H&E: Hematoxylin and eosin; HFD: High-fat diet; PAMV: Portal anterior mesenteric vein.

Myeloperoxidase is another important enzyme secreted by activated macrophages at multiple stages of plaque development. Recently, *in vivo* MRI of myeloperoxidase has been achieved with the development of the gadolinium-based myeloperoxidase sensor bis-5HT-DTPA(Gd) in rabbit atherosclerotic plaques [151]. Lastly, cellular apoptosis is also a key feature of plaque progression and stability. Imaging of apoptosis has been shown in atherosclerotic mice using gadolinium-loaded micelles targeting annexin-5 [152].

■ Assessment of vascular remodeling

Positive remodeling has been recognized as a possible mechanism to alleviate luminal narrowing based on autopsy studies [153–155]. In previous *in vivo* MRI studies of patients with subclinical coronary atherosclerosis [156,157] and of Watanabe hypercholesterolemic rabbits [121], positive remodeling was observed as an increase in the vessel wall area, determined by the outer vessel wall contour, with concurrent preservation of the lumen area. More recently, MRI characterization of vessel wall remodeling and its association with plaque vulnerability, using standardized cut off values, has been shown in atherosclerotic rabbits (Figure 5) [122].

Conclusion & future perspective

Noncontrast-enhanced, contrast-enhanced and molecular MRI of various biological processes in atherosclerosis have been successfully demonstrated in small and large animal models as well as human subjects. The use of animal models allows the development of new imaging

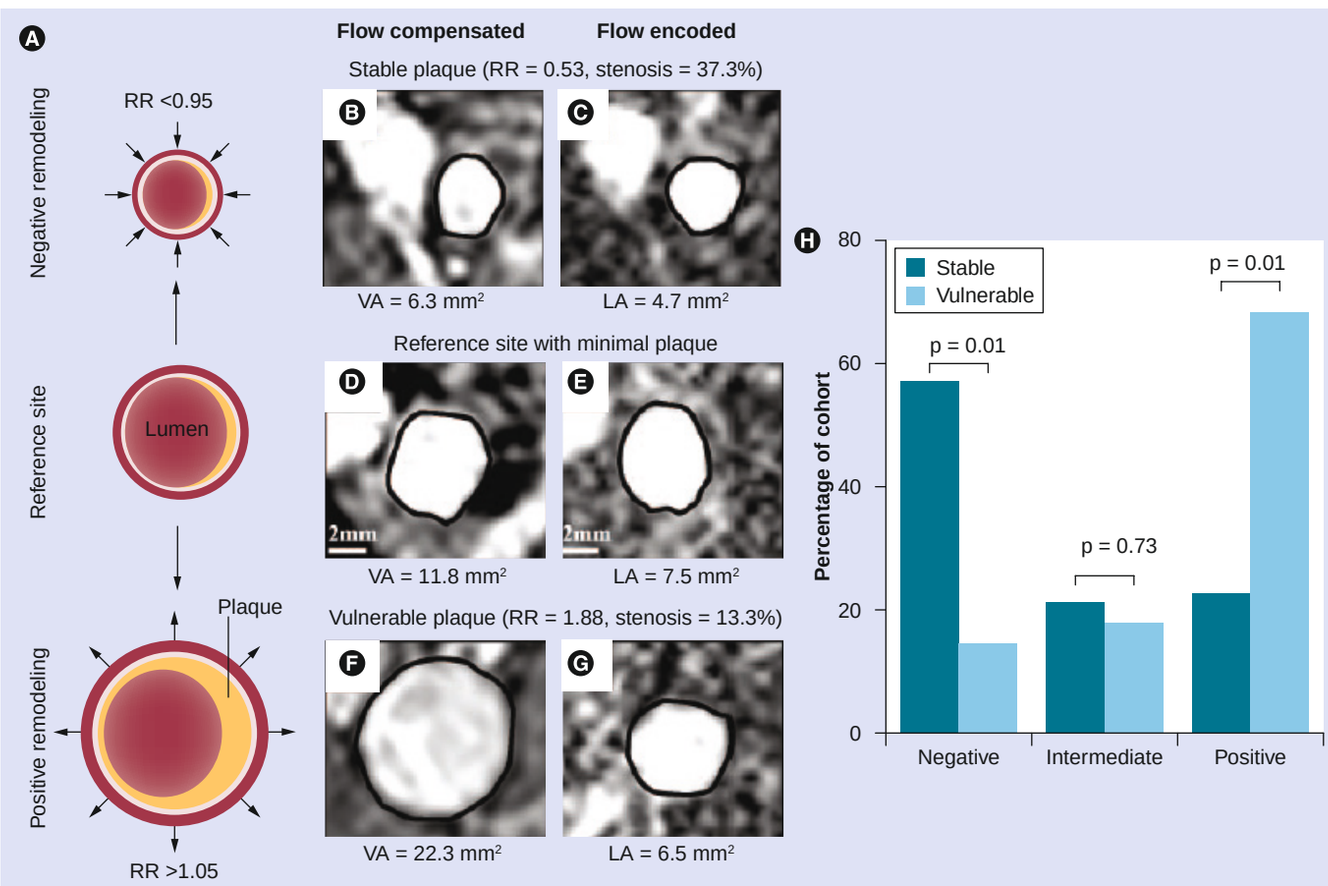

Figure 5. Examples of negative and positive remodeling in stable and vulnerable plaques. (A) Types of vessel wall remodeling. The area circumscribed by the adventitial contour (blue line) indicates the vessel area. The remodeling ratio = VA lesion site/VA reference. The reference site is the site with the least amount of plaque. Positive remodeling and negative remodeling are defined from the remodeling ratio as shown. **(B–G)** Examples of negative and positive remodeling in a stable **(B & C)** and a vulnerable **(F & G)** plaque compared with a reference site **(D & E)**. **(B, D & F)** Flow-compensated images acquired with gadolinium showed negative remodeling at the site of a stable plaque **(B)** and positive remodeling at the site of a vulnerable plaque **(H)**. **(C, E & G)** Flow-encoded images show the unobstructed luminal area. **(H)** Frequency of negative, intermediate and positive remodeling in stable and vulnerable plaques. Negative remodeling was significantly greater in stable plaques whereas positive remodeling was significantly greater in vulnerable plaques. Intermediate remodeling was similar between the two groups [122].
LA: Luminal area; RR: Remodeling ratio; VA: Vessel area.

protocols, contrast agents and therapeutic interventions in a controlled fashion. Furthermore, it provides specimens for *ex vivo* validation studies. The noninvasive nature of MRI, the high spatial resolution and the lack of ionizing radiation make MRI an advantageous imaging modality for both preclinical and clinical studies. The development of higher field scanners and dedicated coils that allow for higher signal:noise ratio, the incorporation of multiple elements in the coils that allow higher acceleration factors, and the ongoing development of pulse sequences can significantly improve the diagnostic performance of MRI and allow translation of the knowledge derived from preclinical studies to imaging of the human disease. The ultimate goal of *in vivo* MRI of atherosclerosis is to reliably and prospectively identify plaques at higher risk for disruption that could improve medical decision making and patient outcome.

Currently, the use of most new contrast agents has been limited to preclinical models for investigating imaging protocols and elucidating the underlying biological processes involved in disease progression in a longitudinal noninvasive manner. Despite the exciting and promising results derived from the preclinical studies very few of these agents progressed to the clinical setting [158,159]. Important limitations that impede the translation to the clinical arena include scalability, cost, safety, favorable pharmacokinetics and regulatory guidelines [160]. Recently, two major prospective clinical studies that examined coronary atherosclerotic vessels in humans revealed that independent predictors including a large plaque burden, a small lumen area and a thin cap fibroatheroma (PROSPECT study) [161] and remodeling index (VIVA study) [162] were associated with future major adverse cardiac events as classified by radiofrequency IVUS. As shown in this review, similar measurements have been derived with native noncontrast and molecular MRI both in a preclinical and clinical setting. Although IVUS has superior spatial resolution compared with MRI it is invasive and therefore not suitable as a screening method. To this end, we envision the future use of noncontrast and molecular MRI as a noninvasive test for risk assessment and monitoring of interventions in subjects with suspected atherosclerosis by morphologic and biological plaque characterization.

Executive summary

Background

- Atherosclerosis and its thrombotic complications are considered the major contributor to the development of acute cardiovascular symptoms.
- Histological studies have added indispensable knowledge to our understanding of the pathophysiology of atherosclerosis but they are limited by their retrospective nature.
- Several invasive and noninvasive imaging modalities have shown the feasibility of *in vivo* vessel wall imaging for the characterization of atherosclerosis.

Animal models of atherosclerosis

- The complexity and slow progression of atherosclerosis in humans and the unpredictable nature of thrombotic events have necessitated the development of several animal models.
- Although no perfect animal model exists, each animal model can be used to address specific biological questions.
- The use of animal models has broadened our understanding of the molecular and cellular pathways involved in disease progression and its clinical complications, the development of new imaging modalities, contrast agents and therapeutic interventions in a controlled fashion.

MRI of atherosclerosis in animal models & humans

- MRI has evolved as one of the leading noninvasive imaging modalities to visualize the vessel wall with high spatial resolution and without ionizing radiation, making it suitable for both preclinical and clinical studies.
- Noncontrast-enhanced, contrast-enhanced and molecular MRI of various biological processes in atherosclerosis has been successfully demonstrated in small and large animal models as well as human subjects.
- Currently, MRI can be used to assess plaque burden and composition, endothelial activation and permeability, plaque enzymatic activity and apoptosis, macrophages and lipoproteins, neovascularization, intraplaque hemorrhage and thrombus, extracellular matrix and vascular remodeling.

Conclusion & future perspective

- The noninvasive nature of MRI, the high spatial resolution and the lack of ionizing radiation make MRI an advantageous modality for imaging atherosclerosis.
- The ongoing optimization of both MRI hardware and software can significantly improve the diagnostic performance of MRI and allow us to translate the knowledge derived from preclinical studies to imaging of the human disease.
- The ultimate goal of *in vivo* MRI of atherosclerosis is to reliably and prospectively identify plaques at higher risk of disruption that could improve medical decision making and patient outcome.

Financial & competing interests disclosure

The authors have no relevant affiliations or financial involvement with any organization or entity with a financial interest in or financial conflict with the subject matter or materials discussed in the manuscript. This includes employment, consultancies, honoraria, stock ownership or options, expert testimony, grants or patents received or pending, or royalties.

No writing assistance was utilized in the production of this manuscript.

References

Papers of special note have been highlighted as:
▪ of interest
▪▪ of considerable interest

1 Anitschkow N. [Über die veränderungen der kaninchenaorta bei experimenteller cholesterinsteatose]. *Beiträge zur Pathologischen Anatomie und zur Allgemeinen Pathologie* 56, 379–404 (1913).

▪▪ **One of the first publications demonstrating that cholesterol-rich diets induce experimental atherosclerosis in rabbits.**

2 Ross R. Atherosclerosis – an inflammatory disease. *N. Engl. J. Med.* 340(2), 115–126 (1999).

3 Lusis AJ. Atherosclerosis. *Nature* 407(6801), 233–241 (2000).

4 Libby P, Ridker PM, Maseri A. Inflammation and atherosclerosis. *Circulation* 105(9), 1135–1143 (2002).

5 Katsuda S, Kaji T. Atherosclerosis and extracellular matrix. *J. Atheroscleros. Thrombos.* 10(5), 267–274 (2003).

6 Krettek A, Sukhova GK, Libby P. Elastogenesis in human arterial disease: a role for macrophages in disordered elastin synthesis. *Arterioscler. Thromb. Vasc. Biol.* 23(4), 582–587 (2003).

7 Lloyd-Jones D, Adams R, Carnethon M *et al.* Heart disease and stroke statistics – 2009 update: a report from the American heart association statistics committee and stroke statistics subcommittee. *Circulation* 119(3), 480–486 (2009).

8 Murray CJ, Lopez AD. Global mortality, disability, and the contribution of risk factors: global burden of disease study. *Lancet* 349(9063), 1436–1442 (1997).

9 Stary HC, Chandler AB, Dinsmore RE *et al.* A definition of advanced types of atherosclerotic lesions and a histological classification of atherosclerosis. A report from the Committee on Vascular Lesions of the Council on Arteriosclerosis, American Heart Association. *Arterioscler. Thromb. Vasc. Biol.* 15(9), 1512–1531 (1995).

10 Stary HC, Chandler AB, Dinsmore RE *et al.* A definition of advanced types of atherosclerotic lesions and a histological classification of atherosclerosis. A report from the Committee on Vascular Lesions of the Council on Arteriosclerosis, American Heart Association. *Circulation* 92(5), 1355–1374 (1995).

11 Stary HC. Natural history and histological classification of atherosclerotic lesions: an update. *Arterioscler. Thromb. Vasc. Biol.* 20(5), 1177–1178 (2000).

12 Virmani R, Kolodgie FD, Burke AP, Farb A, Schwartz SM. Lessons from sudden coronary death: a comprehensive morphological classification scheme for atherosclerotic lesions. *Arterioscler. Thromb. Vasc. Biol.* 20(5), 1262–1275 (2000).

13 Constantinides P. Plaque fissures in human coronary thrombosis. *J. Atheroscler. Res.* 6, 1–17 (1966).

▪▪ **Provided histological evidence that plaque rupture was the underlying cause of most acute cardiovascular events in subjects that have died suddenly.**

14 Burke AP, Farb A, Malcom GT, Liang YH, Smialek J, Virmani R. Coronary risk factors and plaque morphology in men with coronary disease who died suddenly. *N. Engl. J. Med.* 336(18), 1276–1282 (1997).

15 Kolodgie FD, Burke AP, Farb A *et al.* The thin-cap fibroatheroma: a type of vulnerable plaque: the major precursor lesion to acute coronary syndromes. *Curr. Opin. Cardiol.* 16(5), 285–292 (2001).

16 Boyle JJ. Association of coronary plaque rupture and atherosclerotic inflammation. *J. Pathol.* 181(1), 93–99 (1997).

17 van der Wal AC, Becker AE, van der Loos C, Das P. Site of intimal rupture or erosion of thrombosed coronary atherosclerotic plaques is characterized by an inflammatory process irrespective of the dominant plaque morphology. *Circulation* 89, 36–44 (1994).

18 Moreno PR, Purushothaman KR, Sirol M, Levy AP, Fuster V. Neovascularization in human atherosclerosis. *Circulation* 113(18), 2245–2252 (2006).

19 Moreno PR, Purushothaman KR, Fuster V, O'Connor WN. Intimomedial interface damage and adventitial inflammation is increased beneath disrupted atherosclerosis in the aorta: implications for plaque vulnerability. *Circulation* 105(21), 2504–2511 (2002).

20 Kolodgie FD, Gold HK, Burke AP *et al.* Intraplaque hemorrhage and progression of coronary atheroma. *N. Engl. J. Med.* 349(24), 2316–2325 (2003).

21 Pasterkamp G, Schoneveld AH, Hijnen DJ *et al.* Atherosclerotic arterial remodeling and the localization of macrophages and matrix metalloproteases 1, 2 and 9 in the human coronary artery. *Atherosclerosis* 150(2), 245–253 (2000).

22 Farb A, Burke AP, Tang AL *et al.* Coronary plaque erosion without rupture into a lipid core. A frequent cause of coronary thrombosis in sudden coronary death. *Circulation* 93(7), 1354–1363 (1996).

▪▪ **Provided histological evidence that plaque erosion without rupture can cause thrombosis leading to sudden death in humans.**

23 Ambrose JA, Tannenbaum MA, Alexopoulos D *et al.* Angiographic progression of coronary artery disease and the development of myocardial infarction. *J. Am. Coll. Cardiol.* 12(1), 56–62 (1988).

24 Giroud D, Li JM, Urban P, Meier B, Rutishauer W. Relation of the site of acute myocardial infarction to the most severe coronary arterial stenosis at prior angiography. *Am. J. Cardiol.* 69(8), 729–732 (1992).

25 Moise A, Lesperance J, Theroux P, Taeymans Y, Goulet C, Bourassa MG. Clinical and angiographic predictors of new total coronary occlusion in coronary artery disease: analysis of 313 nonoperated patients. *Am. J. Cardiol.* 54(10), 1176–1181 (1984).

26 Anitschkow N, Chalatow S. [Ueber experimentelle cholesterinsteatose und ihre bedeutung für die entstehung einiger pathologischer prozesse.] *Centrbl. Allg. Pathol. Pathol. Anat.* 24, 1–9 (1913).

27 Fayad ZA, Fuster V, Nikolaou K, Becker C. Computed tomography and magnetic resonance imaging for noninvasive coronary angiography and plaque imaging: current and potential future concepts. *Circulation* 106(15), 2026–2034 (2002).

28 Choudhury RP, Fayad ZA. Imaging of atherosclerosis. Coronary wall imaging with MRI. *J. Cardiovasc. Risk* 9(5), 263–270 (2002).

29 Choudhury RP, Fuster V, Badimon JJ, Fisher EA, Fayad ZA. MRI and characterization of atherosclerotic plaque: emerging applications and molecular imaging. *Arterioscler. Thromb. Vasc. Biol.* 22(7), 1065–1074 (2002).

30 Fayad ZA. The assessment of the vulnerable atherosclerotic plaque using MR imaging: a brief review. *Int. J. Cardiovasc. Imag.* 17(3), 165–177 (2001).

31 Fayad ZA. MR imaging for the noninvasive assessment of atherothrombotic plaques. *Magn. Reson. Imaging Clin. N. Am.* 11(1), 101–113 (2003).

32 Fayad ZA, Fuster V. Clinical imaging of the high-risk or vulnerable atherosclerotic plaque. *Circ. Res.* 89(4), 305–316 (2001).

33 Yuan C, Kerwin WS, Yarnykh VL *et al.* MRI of atherosclerosis in clinical trials. *NMR Biomed.* 19(6), 636–654 (2006).

34 Yuan C, Hatsukami TS, Obrien KD. High-resolution magnetic resonance imaging of normal and atherosclerotic human coronary arteries *ex vivo*: discrimination of plaque tissue components. *J. Investig. Med.* 49(6), 491–499 (2001).

35 Fayad ZA, Fuster V, Fallon JT *et al.* Noninvasive *in vivo* human coronary artery lumen and wall imaging using black-blood magnetic resonance imaging. *Circulation* 102(5), 506–510 (2000).

▪▪ **Demonstrated the usefulness of the black-blood pulse sequence for delineation of the vessel wall from the blood and the visualization of atherosclerosis.**

36 Fayad ZA, Fallon JT, Shinnar M *et al.* Noninvasive *in vivo* high-resolution magnetic resonance imaging of atherosclerotic lesions in genetically engineered mice. *Circulation* 98(15), 1541–1547 (1998).

37 Choudhury RP, Aguinaldo JG, Rong JX *et al.* Atherosclerotic lesions in genetically modified mice quantified *in vivo* by non-invasive high-resolution magnetic resonance microscopy. *Atherosclerosis* 162(2), 315–321 (2002).

38 Wiesmann F, Szimtenings M, Frydrychowicz A *et al.* High-resolution MRI with cardiac and respiratory gating allows for accurate *in vivo* atherosclerotic plaque visualization in the murine aortic arch. *Magn. Reson. Med.* 50(1), 69–74 (2003).

39 Itskovich VV, Choudhury RP, Aguinaldo JG *et al.* Characterization of aortic root atherosclerosis in ApoE knockout mice: high-resolution *in vivo* and *ex vivo* MRM with histological correlation. *Magn. Reson. Med.* 49(2), 381–385 (2003).

40 Trogan E, Fayad ZA, Itskovich VV *et al.* Serial studies of mouse atherosclerosis by *in vivo* magnetic resonance imaging detect lesion regression after correction of dyslipidemia. *Arterioscler. Thromb. Vasc. Biol.* 24(9), 1714–1719 (2004).

41 Manka DR, Gilson W, Sarembock I, Ley K, Berr SS. Noninvasive *in vivo* magnetic resonance imaging of injury-induced neointima formation in the carotid artery of the apolipoprotein-E null mouse. *J. Magn. Reson. Imaging* 12(5), 790–794 (2000).

42 Skinner MP, Yuan C, Mitsumori L *et al.* Serial magnetic resonance imaging of experimental atherosclerosis detects lesion fine structure, progression and complications *in vivo*. *Nat. Med.* 1(1), 69–73 (1995).

▪▪ **Initial demonstration of the feasibility to image exeprimental atherosclerosis in rabbits *in vivo*.**

43 Trouard TP, Altbach MI, Hunter GC, Eskelson CD, Gmitro AF. MRI and NMR spectroscopy of the lipids of atherosclerotic plaque in rabbits and humans. *Magn. Reson. Med.* 38(1), 19–26 (1997).

44 McConnell MV, Aikawa M, Maier SE, Ganz P, Libby P, Lee RT. MRI of rabbit atherosclerosis in response to dietary cholesterol lowering. *Arterioscler. Thromb. Vasc. Biol.* 19(8), 1956–1959 (1999).

45 Johnstone MT, Botnar RM, Perez AS *et al.* *In vivo* magnetic resonance imaging of experimental thrombosis in a rabbit model. *Arterioscler. Thromb. Vasc. Biol.* 21(9), 1556–1560 (2001).

▪▪ ***In vivo* identification of thrombosis associated with plaque disruption in rabbits.**

46 Helft G, Worthley SG, Fuster V *et al.* Atherosclerotic aortic component quantification by noninvasive magnetic resonance imaging: an *in vivo* study in rabbits. *J. Am. Coll. Cardiol.* 37(4), 1149–1154 (2001).

47 Helft G, Worthley SG, Fuster V *et al.* Progression and regression of atherosclerotic lesions – monitoring with serial noninvasive magnetic resonance imaging. *Circulation* 105(8), 993–998 (2002).

48 Ronald JA, Walcarius R, Robinson JF, Hegele RA, Rutt BK, Rogers KA. MRI of early- and late-stage arterial remodeling in a low-level cholesterol-fed rabbit model of atherosclerosis. *J. Magn. Reson. Imaging* 26(4), 1010–1019 (2007).

49 Ma X, Zhao Q, Zhao L *et al.* *In vivo* MR imaging of plaque disruption and thrombus formation in an atherosclerotic rabbit model. *Int. J. Cardiovasc. Imaging* doi:10.1007/s11239-006-7861-x (2011) (Epub ahead of print).

50 Yuan C, Skinner MP, Kaneko E *et al.* Magnetic resonance imaging to study lesions of atherosclerosis in the hyperlipidemic rabbit aorta. *Magn. Reson. Imaging* 14(1), 93–102 (1996).

51 Worthley SG, Helft G, Fuster V *et al.* Serial *in vivo* MRI documents arterial remodeling in experimental atherosclerosis. *Circulation* 101(6), 586–589 (2000).

52 Sharma R, Singh RB. MRI of coronary artery atherosclerosis in rabbits: histopathology–MRI correlation and atheroma characterization. *Thromb. J.* 2(1), 5 (2004).

53 Worthley SG, Helft G, Fuster V *et al.* Noninvasive *in vivo* magnetic resonance imaging of experimental coronary artery lesions in a porcine model. *Circulation* 101(25), 2956–2961 (2000).

54 Toussaint JF, Southern JF, Fuster V, Kantor HL. T_2-weighted contrast for NMR characterization of human atherosclerosis. *Arterioscler. Thromb. Vasc. Biol.* 15(10), 1533–1542 (1995).

55 Shinnar M, Fallon JT, Wehrli S *et al.* The diagnostic accuracy of *ex vivo* MRI for human atherosclerotic plaque characterization. *Arterioscler. Thromb. Vasc. Biol.* 19(11), 2756–2761 (1999).

56 Serfaty JM, Chaabane L, Tabib A, Chevallier JM, Briguet A, Douek PC. Atherosclerotic plaques: classification and characterization with T_2-weighted high-spatial-resolution MR imaging – an *in vitro* study. *Radiology* 219(2), 403–410 (2001).

57 Morrisett J, Vick W, Sharma R *et al.* Discrimination of components in atherosclerotic plaques from human carotid endarterectomy specimens by magnetic resonance imaging *ex vivo*. *Magn. Reson. Imaging* 21(5), 465–474 (2003).

58 Rogers WJ, Prichard JW, Hu YL *et al.* Characterization of signal properties in atherosclerotic plaque components by intravascular MRI. *Arterioscler. Thromb. Vasc. Biol.* 20(7), 1824–1830 (2000).

59 Ronen RR, Clarke SE, Hammond RR, Rutt BK. Carotid plaque classification: defining the certainty with which plaque components can be differentiated. *Magn. Reson. Med.* 57(5), 874–880 (2007).

60 Yuan C, Beach KW, Smith LH Jr, Hatsukami TS. Measurement of atherosclerotic carotid plaque size *in vivo* using high resolution magnetic resonance imaging. *Circulation* 98(24), 2666–2671 (1998).

61 Saam T, Ferguson MS, Yarnykh VL *et al.* Quantitative evaluation of carotid plaque composition by *in vivo* MRI. *Arterioscler. Thromb. Vasc. Biol.* 25(1), 234–239 (2005).

62 Yuan C, Mitsumori LM, Ferguson MS *et al.* *In vivo* accuracy of multispectral magnetic resonance imaging for identifying lipid-rich necrotic cores and intraplaque hemorrhage in advanced human carotid plaques. *Circulation* 104(17), 2051–2056 (2001).

▪ **The application of the multicontrast MRI approach to identify different plaque components.**

63 Cai JM, Hatsukami TS, Ferguson MS, Small R, Polissar NL, Yuan C. Classification of human carotid atherosclerotic lesions with *in vivo* multicontrast magnetic resonance imaging. *Circulation* 106(11), 1368–1373 (2002).

64 Mitsumori LM, Hatsukami TS, Ferguson MS, Kerwin WS, Cai J, Yuan C. *In vivo* accuracy of multisequence MR imaging for identifying unstable fibrous caps in advanced human carotid plaques. *J. Magn. Reson. Imaging* 17(4), 410–420 (2003).

65 Kampschulte A, Ferguson MS, Kerwin WS *et al.* Differentiation of intraplaque versus juxtaluminal hemorrhage/thrombus in advanced human carotid atherosclerotic lesions by *in vivo* magnetic resonance imaging. *Circulation* 110(20), 3239–3244 (2004).

66 Chu B, Kampschulte A, Ferguson MS *et al.* Hemorrhage in the atherosclerotic carotid plaque: a high-resolution MRI study. *Stroke* 35(5), 1079–1084 (2004).

67 Saam T, Cai J, Ma L *et al.* Comparison of symptomatic and asymptomatic atherosclerotic carotid plaque features with *in vivo* MR imaging. *Radiology* 240(2), 464–472 (2006).

68 Toussaint JF, Southern JF, Fuster V, Kantor HL. Water diffusion properties of human atherosclerosis and thrombosis measured by pulse field gradient nuclear magnetic resonance. *Arterioscler. Thromb. Vasc. Biol.* 17(3), 542–546 (1997).

69 Qiao Y, Ronen I, Viereck J, Ruberg FL, Hamilton JA. Identification of atherosclerotic lipid deposits by diffusion-weighted imaging. *Arterioscler. Thromb. Vasc. Biol.* 27(6), 1440–1446 (2007).

70 Pachot-Clouard M, Vaufrey F, Darrasse L, Toussainti JF. Magnetization transfer characteristics in atherosclerotic plaque components assessed by adapted binomial preparation pulses. *Magma* 7(1), 9–15 (1998).

71 Wasserman BA, Smith WI, Trout HH 3rd, Cannon RO 3rd, Balaban RS, Arai AE. Carotid artery atherosclerosis: *in vivo* morphologic characterization with gadolinium-enhanced double-oblique MR imaging initial results. *Radiology* 223(2), 566–573 (2002).

72 Kramer CM, Cerilli LA, Hagspiel K, Dimaria JM, Epstein FH, Kern JA. Magnetic resonance imaging identifies the fibrous cap in atherosclerotic abdominal aortic aneurysm. *Circulation* 109(8), 1016–1021 (2004).

73 Cai J, Hatsukami TS, Ferguson MS *et al.* *In vivo* quantitative measurement of intact fibrous cap and lipid-rich necrotic core size in atherosclerotic carotid plaque: comparison of high-resolution, contrast-enhanced magnetic resonance imaging and histology. *Circulation* 112(22), 3437–3444 (2005).

74 Maintz D, Ozgun M, Hoffmeier A *et al.* Selective coronary artery plaque visualization and differentiation by contrast-enhanced inversion prepared MRI. *Eur. Heart J.* 27(14), 1732–1736 (2006).

75 Yeon SB, Sabir A, Clouse M *et al.* Delayed-enhancement cardiovascular magnetic resonance coronary artery wall imaging: comparison with multislice computed tomography and quantitative coronary angiography. *J. Am. Coll. Cardiol.* 50(5), 441–447 (2007).

76 Ibrahim T, Makowski MR, Jankauskas A *et al.* Serial contrast-enhanced cardiac magnetic resonance imaging demonstrates regression of hyperenhancement within the coronary artery wall in patients after acute myocardial infarction. *JACC Cardiovasc. Imaging* 2(5), 580–588 (2009).

77 Botnar RM, Stuber M, Danias PG, Kissinger KV, Manning WJ. A fast 3D approach for coronary MRA. *J. Magn. Reson. Imaging* 10(5), 821–825 (1999).

78 Botnar RM, Stuber M, Danias PG, Kissinger KV, Manning WJ. Improved coronary artery definition with T_2-weighted, free-breathing, three-dimensional coronary MRA. *Circulation* 99(24), 3139–3148 (1999).

▪▪ **Application of advanced pulse sequences for coronary MR angiography.**

79 Stuber M, Botnar RM, Danias PG, Kissinger KV, Manning WJ. Breathhold three-dimensional coronary magnetic resonance angiography using real-time navigator technology. *J. Cardiovasc. Magn. Reson.* 1(3), 233–238 (1999).

80 Stuber M, Botnar RM, Danias PG *et al.* Double-oblique free-breathing high resolution three-dimensional coronary magnetic resonance angiography. *J. Am. Coll. Cardiol.* 34(2), 524–531 (1999).

▪▪ **Application of advanced pulse sequences for coronary MR angiography.**

81 Katoh M, Spuentrup E, Stuber M *et al.* Inversion prepared coronary MR angiography: direct visualization of coronary blood flow. *Rofo* 177(2), 173–178 (2005).

▪▪ **Application of advanced pulse sequences.**

82 Kim WY, Astrup AS, Stuber M *et al.* Subclinical coronary and aortic atherosclerosis detected by magnetic resonance imaging in Type 1 diabetes with and without diabetic nephropathy. *Circulation* 115(2), 228–235 (2007).

83 Pedersen SF, Thrysoe SA, Paaske WP *et al.* CMR assessment of endothelial damage and angiogenesis in porcine coronary arteries using gadofosveset. *J. Cardiovasc. Magn. Reson.* 13, 10 (2011).

84 Kelly KA, Allport JR, Tsourkas A, Shinde-Patil VR, Josephson L, Weissleder R. Detection of vascular adhesion molecule-1 expression using a novel multimodal nanoparticle. *Circ. Res.* 96(3), 327–336 (2005).

85 Nahrendorf M, Jaffer FA, Kelly KA *et al.* Noninvasive vascular cell adhesion molecule-1 imaging identifies inflammatory activation of cells in atherosclerosis. *Circulation* 114(14), 1504–1511 (2006).

86 Mcateer MA, Schneider JE, Ali ZA *et al.* Magnetic resonance imaging of endothelial adhesion molecules in mouse atherosclerosis using dual-targeted microparticles of iron oxide. *Arterioscler. Thromb. Vasc. Biol.* 28(1), 77–83 (2008).

87 van Bochove GS, Paulis LE, Segers D *et al.* Contrast enhancement by differently sized paramagnetic MRI contrast agents in mice with two phenotypes of atherosclerotic plaque. *Contrast Media Mol. Imaging* 6(1), 35–45 (2011).

88 Ruehm SG, Corot C, Vogt P, Kolb S, Debatin JF. Magnetic resonance imaging of atherosclerotic plaque with ultrasmall superparamagnetic particles of iron oxide in hyperlipidemic rabbits. *Circulation* 103(3), 415–422 (2001).

89 Yancy AD, Olzinski AR, Hu TC *et al.* Differential uptake of ferumoxtran-10 and ferumoxytol, ultrasmall superparamagnetic iron oxide contrast agents in rabbit: critical determinants of atherosclerotic plaque labeling. *J. Magn. Reson. Imaging* 21(4), 432–442 (2005).

90 Hyafil F, Laissy JP, Mazighi M *et al.* Ferumoxtran-10-enhanced MRI of the hypercholesterolemic rabbit aorta: relationship between signal loss and macrophage infiltration. *Arterioscler. Thromb. Vasc. Biol.* 26(1), 176–181 (2006).

91 Herborn CU, Vogt FM, Lauenstein TC *et al.* Magnetic resonance imaging of experimental atherosclerotic plaque: comparison of two ultrasmall superparamagnetic particles of iron oxide. *J. Magn. Reson. Imaging* 24(2), 388–393 (2006).

92 Sigovan M, Boussel L, Sulaiman A *et al.* Rapid-clearance iron nanoparticles for inflammation imaging of atherosclerotic plaque: initial experience in animal model. *Radiology* 252(2), 401–409 (2009).

93 Durand E, Raynaud JS, Bruneval P *et al.* Magnetic resonance imaging of ruptured plaques in the rabbit with ultrasmall superparamagnetic particles of iron oxide. *J. Vasc. Res.* 44(2), 119–128 (2007).

94 Korosoglou G, Weiss RG, Kedziorek DA *et al.* Noninvasive detection of macrophage-rich atherosclerotic plaque in hyperlipidemic rabbits using 'positive contrast' magnetic resonance imaging. *J. Am. Coll. Cardiol.* 52(6), 483–491 (2008).

95 Morishige K, Kacher DF, Libby P *et al.* High-resolution magnetic resonance imaging enhanced with superparamagnetic nanoparticles measures macrophage burden in atherosclerosis. *Circulation* 122(17), 1707–1715 (2010).

96 Smith BR, Heverhagen J, Knopp M *et al.* Localization to atherosclerotic plaque and biodistribution of biochemically derivatized superparamagnetic iron oxide nanoparticles (SPIONs) contrast particles for magnetic resonance imaging (MRI). *Biomed. Microdev.* 9(5), 719–727 (2007).

97 Schmitz SA, Winterhalter S, Schiffler S *et al.* USPIO-enhanced direct MR imaging of thrombus: preclinical evaluation in rabbits. *Radiology* 221(1), 237–243 (2001).

98 Makowski MR, Varma G, Wiethoff AJ *et al.* Noninvasive assessment of atherosclerotic plaque progression in ApoE$^{-/-}$ mice using susceptibility gradient mapping. *Circ. Cardiovasc. Imaging* 4(3), 295–303 (2011).

99 Kooi ME, Cappendijk VC, Cleutjens KB *et al.* Accumulation of ultrasmall superparamagnetic particles of iron oxide in human atherosclerotic plaques can be detected by *in vivo* magnetic resonance imaging. *Circulation* 107(19), 2453–2458 (2003).

100 Trivedi RA, U-King-Im JM, Graves MJ, Kirkpatrick PJ, Gillard JH. Noninvasive imaging of carotid plaque inflammation. *Neurology* 63(1), 187–188 (2004).

101 Trivedi RA, U-King-Im JM, Graves MJ *et al.* MRI-derived measurements of fibrous-cap and lipid-core thickness: the potential for identifying vulnerable carotid plaques *in vivo*. *Neuroradiology* 46(9), 738–743 (2004).

102 Trivedi RA, Mallawarachi C, U-King-Im JM *et al.* Identifying inflamed carotid plaques using *in vivo* USPIO-enhanced MR imaging to label plaque macrophages. *Arterioscler. Thromb. Vasc. Biol.* 26(7), 1601–1606 (2006).

103 Tang T, Howarth SP, Miller SR *et al.* Assessment of inflammatory burden contralateral to the symptomatic carotid stenosis using high-resolution ultrasmall, superparamagnetic iron oxide-enhanced MRI. *Stroke* 37(9), 2266–2270 (2006).

104 Tang TY, Howarth SP, Miller SR *et al.* Comparison of the inflammatory burden of truly asymptomatic carotid atheroma with atherosclerotic plaques contralateral to symptomatic carotid stenosis: an ultra small superparamagnetic iron oxide enhanced magnetic resonance study. *J. Neurol. Neurosurg. Psychiat.* 78(12), 1337–1343 (2007).

105 Howarth SP, Tang TY, Trivedi R *et al.* Utility of USPIO-enhanced MR imaging to identify inflammation and the fibrous cap: a comparison of symptomatic and asymptomatic individuals. *Eur. J. Radiol.* 70(3), 555–560 (2009).

106 Amirbekian V, Lipinski MJ, Briley-Saebo KC *et al.* Detecting and assessing macrophages *in vivo* to evaluate atherosclerosis noninvasively using molecular MRI. *Proc. Natl Acad. Sci. USA* 104(3), 961–966 (2007).

107 Mulder WJ, Strijkers GJ, Briley-Saboe KC *et al.* Molecular imaging of macrophages in atherosclerotic plaques using bimodal PEG-micelles. *Magn. Reson. Med.* 58(6), 1164–1170 (2007).

108 Te Boekhorst BC, Bovens SM, Rodrigues-Feo J *et al.* Characterization and *in vitro* and *in vivo* testing of CB2-receptor- and NGAL-targeted paramagnetic micelles for molecular MRI of vulnerable atherosclerotic plaque. *Mol. Imaging Biol.* 12(6), 635–651 (2010).

109 Te Boekhorst BC, Bovens SM, Hellings WE *et al.* Molecular MRI of murine atherosclerotic plaque targeting NGAL: a protein associated with unstable human plaque characteristics. *Cardiovasc. Res.* 89(3), 680–688 (2011).

110 Frias JC, Williams KJ, Fisher EA, Fayad ZA. Recombinant HDL-like nanoparticles: a specific contrast agent for MRI of atherosclerotic plaques. *J. Am. Chem. Soc.* 126(50), 16316–16317 (2004).

111 Cormode DP, Chandrasekar R, Delshad A *et al.* Comparison of synthetic high density lipoprotein (HDL) contrast agents for MR imaging of atherosclerosis. *Bioconjug. Chem.* 20(5), 937–943 (2009).

112 Yamakoshi Y, Qiao H, Lowell AN *et al.* LDL-based nanoparticles for contrast enhanced MRI of atheroplaques in mouse models. *Chem. Commun. (Camb.)* 47(31), 8835–8837 (2011).

113 Li D, Patel AR, Klibanov AL *et al.* Molecular imaging of atherosclerotic plaques targeted to oxidized LDL receptor LOX-1 by SPECT/CT and magnetic resonance. *Circ. Cardiovasc. Imaging* 3(4), 464–472 (2010).

114 Briley-Saebo KC, Shaw PX, Mulder WJ *et al.* Targeted molecular probes for imaging atherosclerotic lesions with magnetic resonance using antibodies that recognize oxidation-specific epitopes. *Circulation* 117(25), 3206–3215 (2008).

115 Aoki S, Aoki K, Ohsawa S, Nakajima H, Kumagai H, Araki T. Dynamic MR imaging of the carotid wall. *J. Magn. Reson. Imaging* 9(3), 420–427 (1999).

116 Kerwin W, Hooker A, Spilker M *et al.* Quantitative magnetic resonance imaging analysis of neovasculature volume in carotid atherosclerotic plaque. *Circulation* 107(6), 851–856 (2003).

▪ **Showed that dynamic contrast-enhanced MRI provides an indication of the extent of neovasculature within carotid atherosclerotic plaque.**

117 Lin W, Abendschein DR, Haacke EM. Contrast-enhanced magnetic resonance angiography of carotid arterial wall in pigs. *J. Magn. Reson. Imaging* 7(1), 183–190 (1997).

118 Yuan C, Kerwin WS, Ferguson MS *et al.* Contrast-enhanced high resolution MRI for atherosclerotic carotid artery tissue characterization. *J. Magn. Reson. Imaging* 15(1), 62–67 (2002).

119 Kerwin WS, O'Brien KD, Ferguson MS, Polissar N, Hatsukami TS, Yuan C. Inflammation in carotid atherosclerotic plaque: a dynamic contrast-enhanced MR imaging study. *Radiology* 241(2), 459–468 (2006).

120 Calcagno C, Cornily JC, Hyafil F *et al.* Detection of neovessels in atherosclerotic plaques of rabbits using dynamic contrast enhanced MRI and ^{18}F-FDG PET. *Arterioscler. Thromb. Vasc. Biol.* 28(7), 1311–1317 (2008).

121 Steen H, Lima JA, Chatterjee S *et al.* High-resolution three-dimensional aortic magnetic resonance angiography and quantitative vessel wall characterization of different atherosclerotic stages in a rabbit model. *Invest. Radiol.* 42(9), 614–621 (2007).

122 Phinikaridou A, Ruberg FL, Hallock KJ *et al.* *In vivo* detection of vulnerable atherosclerotic plaque by MRI in a rabbit model. *Circ. Cardiovasc. Imaging* 3(3), 323–332 (2009).

123 Winter PM, Morawski AM, Caruthers SD *et al.* Molecular imaging of angiogenesis in early-stage atherosclerosis with α(v) β3-integrin-targeted nanoparticles. *Circulation* 108(18), 2270–2274 (2003).

124 Winter PM, Neubauer AM, Caruthers SD *et al.* Endothelial α(v)β3 integrin-targeted fumagillin nanoparticles inhibit angiogenesis in atherosclerosis. *Arterioscler. Thromb. Vasc. Biol.* 26(9), 2103–2109 (2006).

125 Lobbes MB, Heeneman S, Passos VL *et al.* Gadofosveset-enhanced magnetic resonance imaging of human carotid atherosclerotic plaques: a proof-of-concept study. *Investigat. Radiol.* 45(5), 275–281 (2010).

126 Lobbes MB, Miserus RJ, Heeneman S *et al.* Atherosclerosis: contrast-enhanced MR imaging of vessel wall in rabbit model – comparison of gadofosveset and gadopentetate dimeglumine. *Radiology* 250(3), 682–691 (2009).

127 Gomori JM, Grossman RI, Goldberg HI, Zimmerman RA, Bilaniuk LT. Intracranial hematomas: imaging by high-field MR. *Radiology* 157(1), 87–93 (1985).

128 Clark RA, Watanabe AT, Bradley WG Jr, Roberts JD. Acute hematomas: effects of deoxygenation, hematocrit, and fibrin-clot formation and retraction on T_2 shortening. *Radiology* 175(1), 201–206 (1990).

129 Moody AR, Pollock JG, O'Connor AR, Bagnall M. Lower-limb deep venous thrombosis: direct MR imaging of the thrombus. *Radiology* 209(2), 349–355 (1998).

130 Rapoport S, Sostman HD, Pope C, Camputaro CM, Holcomb W, Gore JC. Venous clots: evaluation with MR imaging. *Radiology* 162(2), 527–530 (1987).

131 Moody AR, Murphy RE, Morgan PS *et al.* Characterization of complicated carotid plaque with magnetic resonance direct thrombus imaging in patients with cerebral ischemia. *Circulation* 107(24), 3047–3052 (2003).

132 Corti R, Osende JI, Fayad ZA *et al. In vivo* noninvasive detection and age definition of arterial thrombus by MRI. *J. Am. Coll. Cardiol.* 39(8), 1366–1373 (2002).

▪ **Direct thrombus detection by MRI due to the short T_1 relaxation time of methemoglobin.**

133 Viereck J, Ruberg FL, Qiao Y *et al.* MRI of atherothrombosis associated with plaque rupture. *Arterioscler. Thromb. Vasc. Biol.* 25(1), 240–245 (2005).

134 Botnar RM, Perez AS, Witte S *et al. In vivo* molecular imaging of acute and subacute thrombosis using a fibrin-binding magnetic resonance imaging contrast agent. *Circulation* 109(16), 2023–2029 (2004).

▪▪ ***In vivo* application of a fibrin-targeted contrast agent to visualize thrombosis associated with plaque disruption in a rabbit model.**

135 Winter PM, Cai K, Chen J *et al.* Targeted PARACEST nanoparticle contrast agent for the detection of fibrin. *Magn. Reson. Med.* 56(6), 1384–1388 (2006).

136 Flacke S, Fischer S, Scott MJ *et al.* Novel MRI contrast agent for molecular imaging of fibrin: implications for detecting vulnerable plaques. *Circulation* 104(11), 1280–1285 (2001).

137 Johansson LO, Bjornerud A, Ahlstrom HK, Ladd DL, Fujii DK. A targeted contrast agent for magnetic resonance imaging of thrombus: implications of spatial resolution. *J. Magn. Reson. Imaging* 13(4), 615–618 (2001).

138 Botnar RM, Buecker A, Wiethoff AJ *et al. In vivo* magnetic resonance imaging of coronary thrombosis using a fibrin-binding molecular magnetic resonance contrast agent. *Circulation* 110(11), 1463–1466 (2004).

139 Spuentrup E, Buecker A, Katoh M *et al.* Molecular magnetic resonance imaging of coronary thrombosis and pulmonary emboli with a novel fibrin-targeted contrast agent. *Circulation* 111(11), 1377–1382 (2005).

140 Spuentrup E, Fausten B, Kinzel S *et al.* Molecular magnetic resonance imaging of atrial clots in a swine model. *Circulation* 112(3), 396–399 (2005).

141 Spuentrup E, Katoh M, Wiethoff AJ *et al.* Molecular magnetic resonance imaging of pulmonary emboli with a fibrin-specific contrast agent. *Am. J. Respir. Crit. Care Med.* 172(4), 494–500 (2005).

142 Stracke CP, Katoh M, Wiethoff AJ, Parsons EC, Spangenberg P, Spuntrup E. Molecular MRI of cerebral venous sinus thrombosis using a new fibrin-specific MR contrast agent. *Stroke* 38(5), 1476–1481 (2007).

143 Sirol M, Aguinaldo JG, Graham PB *et al.* Fibrin-targeted contrast agent for improvement of *in vivo* acute thrombus detection with magnetic resonance imaging. *Atherosclerosis* 182(1), 79–85 (2005).

144 Spuentrup E, Botnar RM, Wiethoff AJ *et al.* MR imaging of thrombi using EP-2104R, a fibrin-specific contrast agent: initial results in patients. *Eur. Radiol.* 18(9), 1995–2005 (2008).

145 Johansson LO, Bjornerud A, Ahlstrom HK, Ladd DL, Fujii DK. A targeted contrast agent for magnetic resonance imaging of thrombus: implications of spatial resolution. *J. Magn. Reson. Imaging* 13(4), 615–618 (2001).

146 Klink A, Lancelot E, Ballet S *et al.* Magnetic resonance molecular imaging of thrombosis in an arachidonic acid mouse model using an activated platelet targeted probe. *Arterioscler. Thromb. Vasc. Biol.* 30(3), 403–410 (2010).

147 Miserus RJ, Herias MV, Prinzen L *et al.* Molecular MRI of early thrombus formation using a bimodal α2-antiplasmin-based contrast agent. *JACC Cardiovasc. Imaging* 2(8), 987–996 (2009).

148 Makowski MR, Wiethoff AJ, Blume U *et al.* Assessment of atherosclerotic plaque burden with an elastin-specific magnetic resonance contrast agent. *Nat. Med.* 17(3), 383–388 (2011).

▪▪ ***In vivo* application of a new MRI contrast agent that binds specifically to elastin to assess plaque progression.**

149 von Bary C, Makowski M, Preissel A *et al.* MRI of coronary wall remodeling in a swine model of coronary injury using an elastin-binding contrast agent. *Circ. Cardiovasc. Imaging* 4(2), 147–155 (2011).

150 Lancelot E, Amirbekian V, Brigger I *et al.* Evaluation of matrix metalloproteinases in atherosclerosis using a novel noninvasive imaging approach. *Arterioscler. Thromb. Vasc. Biol.* 28(3), 425–432 (2008).

151 Ronald JA, Chen JW, Chen Y *et al.* Enzyme-sensitive magnetic resonance imaging targeting myeloperoxidase identifies active inflammation in experimental rabbit atherosclerotic plaques. *Circulation* 120(7), 592–599 (2009).

152 van Tilborg GA, Vucic E, Strijkers GJ *et al.* Annexin A5-functionalized bimodal nanoparticles for MRI and fluorescence imaging of atherosclerotic plaques. *Bioconjug. Chem.* 21(10), 1794–1803 (2010).

153 Crawford T, Levene CI. Medial thinning in atheroma. *J. Pathol. Bacteriol.* 66(1), 19–23 (1953).

154 Bond MG, Adams MR, Bullock BC. Complicating factors in evaluating coronary artery atherosclerosis. *Artery* 9(1), 21–29 (1981).

155 Glagov S, Weisenberg E, Zarins CK, Stankunavicius R, Kolettis GJ. Compensatory enlargement of human atherosclerotic coronary arteries. *N. Engl. J. Med.* 316(22), 1371–1375 (1987).

▪▪ **Showed that human coronary arteries enlarge in relation to plaque area and that luminal stenosis may be delayed until the lesion occupies 40% of the internal elastic lamina area.**

156 Kim WY, Stuber M, Bornert P, Kissinger KV, Manning WJ, Botnar RM. Three-dimensional black-blood cardiac magnetic resonance coronary vessel wall imaging detects positive arterial remodeling in patients with nonsignificant coronary artery disease. *Circulation* 106(3), 296–299 (2002).

▪▪ **Showed that coronary MRI can be used to detect a Glagov type of arterial remodeling *in vivo*.**

157 Miao C, Chen S, Macedo R *et al.* Positive remodeling of the coronary arteries detected by magnetic resonance imaging in an asymptomatic population: MESA (Multi-Ethnic Study of Atherosclerosis). *J. Am. Coll. Cardiol.* 53(18), 1708–1715 (2009).

158 Tang TY, Howarth SP, Miller SR *et al.* The ATHEROMA (Atorvastatin Therapy: Effects on Reduction of Macrophage Activity) study. Evaluation using ultrasmall superparamagnetic iron oxide-enhanced magnetic resonance imaging in carotid disease. *J. Am. Coll. Cardiol.* 53(22), 2039–2050 (2009).

159 Vymazal J, Spuentrup E, Cardenas-Molina G *et al.* Thrombus imaging with fibrin-specific gadolinium-based MR contrast agent EP-2104R: results of a Phase 2 clinical study of feasibility. *Investigat. Radiol.* 44(11), 697–704 (2009).

160 Buxton DB, Antman M, Danthi N *et al.* Report of the National Heart, Lung, and Blood Institute working group on the translation of cardiovascular molecular imaging. *Circulation* 123(19), 2157–2163 (2011).

161 Stone GW, Maehara A, Lansky AJ *et al.* A prospective natural-history study of coronary atherosclerosis. *N. Engl. J. Med.* 364(3), 226–235 (2011).

162 Calvert PA, Obaid DR, O'Sullivan M *et al.* Association between IVUS findings and adverse outcomes in patients with coronary artery disease: the VIVA (VH-IVUS in vulnerable atherosclerosis) study. *J. Am. Coll. Cardiol. Imaging* 4(8), 894–901 (2011).

163 Paigen B, Holmes PA, Mitchell D, Albee D. Comparison of atherosclerotic lesions and HDL-lipid levels in male, female, and testosterone-treated female mice from strains C57BL/6, BALB/c, and C3H. *Atherosclerosis* 64(2–3), 215–221 (1987).

164 Stewart-Phillips JL, Lough J. Pathology of atherosclerosis in cholesterol-fed, susceptible mice. *Atherosclerosis* 90(2–3), 211–218 (1991).

165 Purcell-Huynh DA, Farese RV Jr, Johnson DF *et al.* Transgenic mice expressing high levels of human apolipoprotein B develop severe atherosclerotic lesions in response to a high-fat diet. *J. Clin. Invest.* 95(5), 2246–2257 (1995).

166 Zhang SH, Reddick RL, Piedrahita JA, Maeda N. Spontaneous hypercholesterolemia and arterial lesions in mice lacking apolipoprotein E. *Science* 258(5081), 468–471 (1992).

167 Plump AS, Smith JD, Hayek T *et al.* Severe hypercholesterolemia and atherosclerosis in apolipoprotein E-deficient mice created by homologous recombination in ES cells. *Cell* 71(2), 343–353 (1992).

168 Reddick RL, Zhang SH, Maeda N. Atherosclerosis in mice lacking apo E. Evaluation of lesional development and progression. *Arterioscler. Thromb.* 14(1), 141–147 (1994).

169 Nakashima Y, Plump AS, Raines EW, Breslow JL, Ross R. ApoE-deficient mice develop lesions of all phases of atherosclerosis throughout the arterial tree. *Arterioscler. Thromb.* 14(1), 133–140 (1994).

170 Rosenfeld ME, Polinsky P, Virmani R, Kauser K, Rubanyi G, Schwartz SM. Advanced atherosclerotic lesions in the innominate artery of the ApoE knockout mouse. *Arterioscler. Thromb. Vasc. Biol.* 20(12), 2587–2592 (2000).

171 Cheng C, Tempel D, Van Haperen R *et al.* Shear stress-induced changes in atherosclerotic plaque composition are modulated by chemokines. *J. Clin. Investigat.* 117(3), 616–626 (2007).

172 Ding SF, Ni M, Liu XL *et al.* A causal relationship between shear stress and atherosclerotic lesions in apolipoprotein E knockout mice assessed by ultrasound biomicroscopy. *Am. J. Physiol. Heart Circ. Physiol.* 298(6), H2121–H2129 (2010).

173 Lutgens E, Daemen M, Kockx M *et al.* Atherosclerosis in APOE*3-leiden transgenic mice: from proliferative to atheromatous stage. *Circulation* 99(2), 276–283 (1999).

174 Ishibashi S, Goldstein JL, Brown MS, Herz J, Burns DK. Massive xanthomatosis and atherosclerosis in cholesterol-fed low density lipoprotein receptor-negative mice. *J. Clin. Invest.* 93(5), 1885–1893 (1994).

175 Powell-Braxton L, Veniant M, Latvala RD *et al.* A mouse model of human familial hypercholesterolemia: markedly elevated low density lipoprotein cholesterol levels and severe atherosclerosis on a low-fat chow diet. *Nat. Med.* 4(8), 934–938 (1998).

176 Sanan DA, Newland DL, Tao R *et al.* Low density lipoprotein receptor-negative mice expressing human apolipoprotein B-100 develop complex atherosclerotic lesions on a chow diet: no accentuation by apolipoprotein(a). *Proc. Natl Acad. Sci. USA* 95(8), 4544–4549 (1998).

177 Masucci-Magoulas L, Goldberg IJ, Bisgaier CL *et al.* A mouse model with features of familial combined hyperlipidemia. *Science* 275(5298), 391–394 (1997).

178 Ishibashi S, Herz J, Maeda N, Goldstein JL, Brown MS. The two-receptor model of lipoprotein clearance: tests of the hypothesis in 'knockout' mice lacking the low density lipoprotein receptor, apolipoprotein E, or both proteins. *Proc. Natl Acad. Sci. USA* 91(10), 4431–4435 (1994).

179 Van Herck JL, De Meyer GR, Martinet W *et al.* Impaired fibrillin-1 function promotes features of plaque instability in apolipoprotein E-deficient mice. *Circulation* 120(24), 2478–2487 (2009).

180 Lemaitre V, O'Byrne TK, Borczuk AC, Okada Y, Tall AR, D'Armiento J. ApoE knockout mice expressing human matrix metalloproteinase-1 in macrophages have less advanced atherosclerosis. *J. Clin. Invest.* 107(10), 1227–1234 (2001).

181 Kuhlencordt PJ, Gyurko R, Han F *et al.* Accelerated atherosclerosis, aortic aneurysm formation, and ischemic heart disease in apolipoprotein E/endothelial nitric oxide synthase double-knockout mice. *Circulation* 104(4), 448–454 (2001).

182 Kuhlencordt PJ, Chen J, Han F, Astern J, Huang PL. Genetic deficiency of inducible nitric oxide synthase reduces atherosclerosis and lowers plasma lipid peroxides in apolipoprotein E-knockout mice. *Circulation* 103(25), 3099–3104 (2001).

183 Welch CL, Sun Y, Arey BJ *et al.* Spontaneous atherothrombosis and medial degradation in ApoE$^{-/-}$, Npc1$^{-/-}$ mice. *Circulation* 116(21), 2444–2452 (2007).

184 Page IH, Brown HB. Induced hypercholesterolemia and atherogenesis. *Circulation* 6(5), 681–687 (1952).

185 Malinow MR, Hojman D, Pellegrino A. Different methods for the experimental production of generalized atherosclerosis in the rat. *Acta Cardiol.* 9(5), 480–499 (1954).

186 Constantinides P. *Experimental Atherosclerosis.* Elsevier Publishing Co., NY, USA (1965).

187 Constantinides P, Gutmann-Auersperg N, Hospes D. Acceleration of intimal atherogenesis through prior medial injury. *AMA Arch. Pathol.* 66(3), 247–254 (1958).

188 Constantinides P, Booth J, Carlson G. Production of advanced cholesterol atherosclerosis in the rabbit. *Arch. Pathol.* 70, 80–92 (1960).

189 Weidinger FF, McLenachan JM, Cybulsky MI *et al.* Hypercholesterolemia enhances macrophage recruitment and dysfunction of regenerated endothelium after balloon injury of the rabbit iliac artery. *Circulation* 84(2), 755–767 (1991).

190 Abela GS, Picon PD, Friedl SE *et al.* Triggering of plaque disruption and arterial thrombosis in an atherosclerotic rabbit model. *Circulation* 91(3), 776–784 (1995).

191 Phinikaridou A, Hallock KJ, Qiao Y, Hamilton JA. A robust rabbit model of human atherosclerosis and atherothrombosis. *J. Lipid Res.* 50(5), 787–797 (2009).

192 Watanabe Y. Serial inbreeding of rabbits with hereditary hyperlipidemia (WHHL-rabbit). *Atherosclerosis* 36(2), 261–268 (1980).

193 Havel RJ, Kita T, Kotite L *et al.* Concentration and composition of lipoproteins in blood plasma of the WHHL rabbit. An animal model of human familial hypercholesterolemia. *Arteriosclerosis* 2(6), 467–474 (1982).

194 Kita T, Goldstein JL, Brown MS, Watanabe Y, Hornick CA, Havel RJ. Hepatic uptake of chylomicron remnants in WHHL rabbits: a mechanism genetically distinct from the low density lipoprotein receptor. *Proc. Natl Acad. Sci. USA* 79(11), 3623–3627 (1982).

195 Buja LM, Kita T, Goldstein JL, Watanabe Y, Brown MS. Cellular pathology of progressive atherosclerosis in the WHHL rabbit. An animal model of familial hypercholesterolemia. *Arteriosclerosis* 3(1), 87–101 (1983).

196 Seddon AM, Woolf N, La Ville A *et al.* Hereditary hyperlipidemia and atherosclerosis in the rabbit due to overproduction of lipoproteins. II. Preliminary report of arterial pathology. *Arteriosclerosis* 7(2), 113–124 (1987).

197 Fox R. *Handbook on Genetically Standardized JAX Rabbit*. Jackson Laboratory, Bar Harbor, ME, USA (1975).

198 Overturf ML, Smith SA, Hewett-Emmett D *et al.* Development and partial metabolic characterization of a dietary cholesterol-resistant colony of rabbits. *J. Lipid Res.* 30(2), 263–273 (1989).

199 Brousseau ME, Hoeg JM. Transgenic rabbits as models for atherosclerosis research. *J. Lipid Res.* 40(3), 365–375 (1999).

200 Tjwa M, Carmeliet P, Moons L. Novel transgenic rabbit model sheds light on the puzzling role of matrix metalloproteinase-12 in atherosclerosis. *Circulation* 113(16), 1929–1932 (2006).

201 Ratcliffe HL, Luginbuhl H. The domestic pig: a model for experimental atherosclerosis. *Atherosclerosis* 13(1), 133–136 (1971).

202 Lee KT, Lee WM. Advanced coronary atherosclerosis in swine produced by combination of balloon-catheter injury and cholesterol feeding. In: *Atherosclerosis: Metabolic, Morphologic and Clinical Aspects*. Manning GW, Haust MD (Eds). Plenum Press, NY, USA, 597–602 (1977).

203 Cevallos WH, Holmes WL, Myers RN, Smink RD. Swine in atherosclerosis research – development of an experimental animal model and study of the effect of dietary fats on cholesterol metabolism. *Atherosclerosis* 34(3), 303–317 (1979).

204 Reitman JS, Mahley RW, Fry DL. Yucatan miniature swine as a model for diet-induced atherosclerosis. *Atherosclerosis* 43(1), 119–132 (1982).

205 Phillips RW, Westmoreland N, Panepinto L, Case GL. Dietary effects on metabolism of Yucatan miniature swine selected for low and high glucose utilization. *J. Nutr.* 112(1), 104–111 (1982).

206 Phillips RW, Panepinto LM, Spangler R, Westmoreland N. Yucatan miniature swine as a model for the study of human diabetes mellitus. *Diabetes* 31(Suppl. 1 Pt 2), S30–S36 (1982).

207 Gerrity RG, Natarajan R, Nadler JL, Kimsey T. Diabetes-induced accelerated atherosclerosis in swine. *Diabetes* 50(7), 1654–1665 (2001).

208 Rapacz J, Hasler-Rapacz J, Taylor KM, Checovich WJ, Attie AD. Lipoprotein mutations in pigs are associated with elevated plasma cholesterol and atherosclerosis. *Science* 234(4783), 1573–1577 (1986).

209 Hasler-Rapacz J, Ellegren H, Fridolfsson AK *et al.* Identification of a mutation in the low density lipoprotein receptor gene associated with recessive familial hypercholesterolemia in swine. *Am. J. Med. Genet.* 76(5), 379–386 (1998).

210 Prescott MF, McBride CH, Hasler-Rapacz J, Von Linden J, Rapacz J. Development of complex atherosclerotic lesions in pigs with inherited hyper-LDL cholesterolemia bearing mutant alleles for apolipoprotein B. *Am. J. Pathol.* 139(1), 139–147 (1991).

211 Thim T, Hagensen MK, Drouet L *et al.* Familial hypercholesterolaemic downsized pig with human-like coronary atherosclerosis: a model for preclinical studies. *Eur. Intervent.* 6(2), 261–268 (2010).

212 Steiner A, Kendall FE. Atherosclerosis and arteriosclerosis in dogs following ingestion of cholesterol and thiouracil. *Arch. Pathol. (Chic.)* 42(4), 433–444 (1946).

213 Luzio NR, O'Neal RM. The rapid development of arterial lesions in dogs fed an infarct-producing diet. *Exp. Mol. Pathol.* 1, 122–132 (1962).

214 Chaabane L, Pellet N, Bourdillon MC *et al.* Contrast enhancement in atherosclerosis development in a mouse model: *in vivo* results at 2 Tesla. *Magma* 17(3–6), 188–195 (2004).

215 Alsaid H, Sabbah M, Bendahmane Z *et al.* High-resolution contrast-enhanced MRI of atherosclerosis with digital cardiac and respiratory gating in mice. *Magn. Reson. Med.* 58(6), 1157–1163 (2007).

216 Hockings PD, Roberts T, Galloway GJ *et al.* Repeated three-dimensional magnetic resonance imaging of atherosclerosis development in innominate arteries of low-density lipoprotein receptor-knockout mice. *Circulation* 106(13), 1716–1721 (2002).

217 Meding J, Urich M, Licha K *et al.* Magnetic resonance imaging of atherosclerosis by targeting extracellular matrix deposition with Gadofluorine M. *Contrast Media Mol. Imaging* 2(3), 120–129 (2007).

218 Barkhausen J, Ebert W, Heyer C, Debatin JF, Weinmann HJ. Detection of atherosclerotic plaque with gadofluorine-enhanced magnetic resonance imaging. *Circulation* 108(5), 605–609 (2003).

219 Sirol M, Itskovich VV, Mani V *et al.* Lipid-rich atherosclerotic plaques detected by gadofluorine-enhanced *in vivo* magnetic resonance imaging. *Circulation* 109(23), 2890–2896 (2004).

220 Sirol M, Moreno PR, Purushothaman KR *et al.* Increased neovascularization in advanced lipid-rich atherosclerotic lesions detected by gadofluorine-M-enhanced MRI: implications for plaque vulnerability. *Circ. Cardiovasc. Imaging* 2(5), 391–396 (2009).

221 Ronald JA, Chen Y, Belisle AJL *et al.* Comparison of gadofluorine-M and Gd-DTPA for noninvasive staging of atherosclerotic plaque stability using MRI. *Circ. Cardiovasc. Imaging* 2(3), 226–234 (2009).

222 Sirol M, Fuster V, Badimon JJ *et al.* Chronic thrombus detection with *in vivo* magnetic resonance imaging and a fibrin-targeted contrast agent. *Circulation* 112(11), 1594–1600 (2005).

223 Hyafil F, Vucic E, Cornily JC *et al.* Monitoring of arterial wall remodelling in atherosclerotic rabbits with a magnetic resonance imaging contrast agent binding to matrix metalloproteinases. *Eur. Heart J.* 32(12), 1561–1571 (2011).

224 Cornily JC, Hyafil F, Calcagno C *et al.* Evaluation of neovessels in atherosclerotic plaques of rabbits using an albumin-binding intravascular contrast agent and MRI. *J. Magn. Reson. Imaging* 27(6), 1406–1411 (2008).

225 Brushett C, Qiu B, Atalar E, Yang X. High-resolution MRI of deep-seated atherosclerotic arteries using motexafin gadolinium. *J. Magn. Reson. Imaging* 27(1), 246–250 (2008).

226 Toussaint JF, Lamuraglia GM, Southern JF, Fuster V, Kantor HL. Magnetic resonance images lipid, fibrous, calcified, hemorrhagic, and thrombotic components of human atherosclerosis *in vivo*. *Circulation* 94(5), 932–938 (1996).

227 Yuan C, Zhang SX, Polissar NL *et al.* Identification of fibrous cap rupture with magnetic resonance imaging is highly associated with recent transient ischemic attack or stroke. *Circulation* 105(2), 181–185 (2002).

228 Yuan C, Zhao XQ, Hatsukami TS. Quantitative evaluation of carotid atherosclerotic plaques by magnetic resonance imaging. *Curr. Atheroscler. Rep.* 4(5), 351–357 (2002).

229 Zhang S, Hatsukami TS, Polissar NL, Han C, Yuan C. Comparison of carotid vessel wall area measurements using three different contrast-weighted black blood MR imaging techniques. *Magn. Reson. Imaging* 19(6), 795–802 (2001).

230 Hatsukami TS, Ross R, Polissar NL, Yuan C. Visualization of fibrous cap thickness and rupture in human atherosclerotic carotid plaque *in vivo* with high-resolution magnetic resonance imaging. *Circulation* 102(9), 959–964 (2000).

231 Ota H, Yu W, Underhill HR *et al.* Hemorrhage and large lipid-rich necrotic cores are independently associated with thin or ruptured fibrous caps: an *in vivo* 3T MRI study. *Arterioscler. Thromb. Vasc. Biol.* 29(10), 1696–1701 (2009).

232 Saam T, Yuan C, Chu B *et al.* Predictors of carotid atherosclerotic plaque progression as measured by noninvasive magnetic resonance imaging. *Atherosclerosis* 194(2), e34–e42 (2007).

233 Takaya N, Yuan C, Chu B *et al.* Presence of intraplaque hemorrhage stimulates progression of carotid atherosclerotic plaques: a high-resolution magnetic resonance imaging study. *Circulation* 111(21), 2768–2775 (2005).

234 Takaya N, Yuan C, Chu B *et al.* Association between carotid plaque characteristics and subsequent ischemic cerebrovascular events: a prospective assessment with MRI – initial results. *Stroke* 37(3), 818–823 (2006).

235 Saam T, Underhill HR, Chu B *et al.* Prevalence of American Heart Association type 6 carotid atherosclerotic lesions identified by magnetic resonance imaging for different levels of stenosis as measured by duplex ultrasound. *J. Am. Coll. Cardiol.* 51(10), 1014–1021 (2008).

236 Underhill HR, Yuan C, Yarnykh VL *et al.* Predictors of surface disruption with MR imaging in asymptomatic carotid artery stenosis. *Am. J. Neuroradiol.* 31(3), 487–493 (2010).

▪ **Prospective investigation of asymptomatic individuals with 50–79% stenosis; provided evidence that the size of the lipid-rich necrotic core may govern the risk of future surface disruption.**

237 Wasserman BA, Astor BC, Sharrett AR, Swingen C, Catellier D. MRI measurements of carotid plaque in the atherosclerosis risk in communities (ARIC) study: methods, reliability and descriptive statistics. *J. Magn. Reson. Imaging* 31(2), 406–415 (2010).

238 Astor BC, Sharrett AR, Coresh J, Chambless LE, Wasserman BA. Remodeling of carotid arteries detected with MR imaging: atherosclerosis risk in communities carotid MRI study. *Radiology* 256(3), 879–886 (2010).

239 Wasserman BA, Wityk RJ, Trout HH 3rd, Virmani R. Low-grade carotid stenosis: looking beyond the lumen with MRI. *Stroke* 36(11), 2504–2513 (2005).

240 Wasserman BA, Casal SG, Astor BC, Aletras AH, Arai AE. Wash-in kinetics for gadolinium-enhanced magnetic resonance imaging of carotid atheroma. *J. Magn. Reson. Imaging* 21(1), 91–95 (2005).

241 Kerwin WS, O'Brien KD, Ferguson MS, Polissar N, Hatsukami TS, Yuan C. Inflammation in carotid atherosclerotic plaque: a dynamic contrast-enhanced MR imaging study. *Radiology* 241(2), 459–468 (2006).

242 Kerwin WS, Oikawa M, Yuan C, Jarvik GP, Hatsukami TS. MR imaging of adventitial vasa vasorum in carotid atherosclerosis. *Magn. Reson. Med.* 59(3), 507–514 (2008).

243 Kerwin WS, Zhao X, Yuan C, Hatsukami TS, Maravilla KR, Underhill HR. Contrast-enhanced MRI of carotid atherosclerosis: dependence on contrast agent. *J. Magn. Reson. Imaging* 30(1), 35–40 (2009).

244 Underhill HR, Yuan C, Yarnykh VL *et al.* Arterial remodeling in [corrected] subclinical carotid artery disease. *JACC Cardiovasc. Imaging* 2(12), 1381–1389 (2009).

245 Murphy RE, Moody AR, Morgan PS *et al.* Prevalence of complicated carotid atheroma as detected by magnetic resonance direct thrombus imaging in patients with suspected carotid artery stenosis and previous acute cerebral ischemia. *Circulation* 107(24), 3053–3058 (2003).

246 Fayad ZA, Nahar T, Fallon JT *et al. In vivo* magnetic resonance evaluation of atherosclerotic plaques in the human thoracic aorta: a comparison with transesophageal echocardiography. *Circulation* 101(21), 2503–2509 (2000).

247 Summers RM, Andrasko-Bourgeois J, Feuerstein IM *et al.* Evaluation of the aortic root by MRI: insights from patients with homozygous familial hypercholesterolemia. *Circulation* 98(6), 509–518 (1998).

248 Jaffer FA, O'Donnell CJ, Larson MG *et al.* Age and sex distribution of subclinical aortic atherosclerosis: a magnetic resonance imaging examination of the Framingham Heart Study. *Arterioscler. Thromb. Vasc. Biol.* 22(5), 849–854 (2002).

249 Taniguchi H, Momiyama Y, Fayad ZA *et al. In vivo* magnetic resonance evaluation of associations between aortic atherosclerosis and both risk factors and coronary artery disease in patients referred for coronary angiography. *Am. Heart J.* 148(1), 137–143 (2004).

250 Botnar RM, Stuber M, Kissinger KV, Kim WY, Spuentrup E, Manning WJ. Noninvasive coronary vessel wall and plaque imaging with magnetic resonance imaging. *Circulation* 102(21), 2582–2587 (2000).

251 Botnar RM, Kim WY, Bornert P, Stuber M, Spuentrup E, Manning WJ. 3D coronary vessel wall imaging utilizing a local inversion technique with spiral image acquisition. *Magn. Reson. Med.* 46(5), 848–854 (2001).

▪▪ **Application of advanced pulse sequences for coronary vessel wall MRI.**

252 Botnar RM, Stuber M, Lamerichs R *et al.* Initial experiences with *in vivo* right coronary artery human MR vessel wall imaging at 3 tesla. *J. Cardiovasc. Magn. Reson.* 5(4), 589–594 (2003).

▪▪ **Application of advanced pulse sequences for coronary vessel wall MRI.**

253 Katoh M, Spuentrup E, Buecker A, Manning WJ, Gunther RW, Botnar RM. MR coronary vessel wall imaging: comparison between radial and spiral k-space sampling. *J. Magn. Reson. Imaging* 23(5), 757–762 (2006).

254 Katoh M, Spuentrup E, Buecker A *et al.* MRI of coronary vessel walls using radial k-space sampling and steady-state free precession imaging. *Am. J. Roentgenol.* 186(6 Suppl. 2), S401–S406 (2006).

255 Jansen CH, Perera D, Makowski MR *et al.* Detection of intracoronary thrombus by magnetic resonance imaging in patients with acute myocardial infarction. *Circulation* 124(4), 416–424 (2011).

256 Stuber M, Botnar RM, Danias PG *et al.* Contrast agent-enhanced, free-breathing, three-dimensional coronary magnetic resonance angiography. *J. Magn. Reson. Imaging* 10(5), 790–799 (1999).